Physica D 471 (2025) 134427

Contents lists available at ScienceDirect

Physica D

journal homepage: www.elsevier.com/locate/physd

Weakly nonlinear analysis of minimal models for Turing patterns

F.R. Waters [a,b,*], C.A. Yates [a,b], J.H.P. Dawes [a]

[a] Department of Mathematical Sciences, University of Bath, Claverton Down, BA2 7AY, UK
[b] Centre for Mathematical Biology, University of Bath, Claverton Down, BA2 7AY, UK

ARTICLE INFO

Communicated by R. Kuske

Keywords:
Pattern formation
Bifurcation
Reaction–diffusion system
Amplitude equation

ABSTRACT

The simplest particle-based mass-action models for Turing instability – i.e. those with only two component species undergoing instantaneous interactions of at most two particles, with the smallest number of distinct interactions – fall into a surprisingly small number of classes of reaction schemes. In previous work we have computed this classification, with different schemes distinguished by the structure of the interactions. Within a given class the reaction stoichiometry and rates remain as parameters that determine the linear and nonlinear evolution of the system.

Adopting the usual weakly nonlinear scalings and analysis reveals that, under suitable choices of reaction stoichiometry, and in nine of the 11 classes of minimal scheme exhibiting a spatially in-phase ("true activator-inhibitor") Turing instability, stable patterns are indeed generated in open regions of parameter space via a generically supercritical bifurcation from the spatially uniform state. In three of these classes the instability is always supercritical while in six there is an open region in which it is subcritical. Intriguingly, however, in the remaining two classes of minimal scheme we require different weakly nonlinear scalings, since the coefficient in the usual cubic normal form unexpectedly vanishes identically. In these cases, a different set of asymptotic scalings is required.

We present a complete analysis through deriving the normal form for these two cases also, which involves quintic terms. This fifth-order normal form also captures the behaviour along the boundaries between the supercritical and subcritical cases of the cubic normal form. The details of these calculations reveal the distinct roles played by reaction rate parameters as compared to stoichiometric parameters.

We quantitatively validate our analysis via numerical simulations and confirm the two different scalings for the amplitude of predicted stable patterned states.

Introduction

Since the highly-cited initial exploration by Alan Turing [1], there has been huge interest, across many scientific fields, in understanding mechanisms for the spontaneous emergence, out of homogeneous equilibrium states, of structure and spatial patterns. The emergence of structure from spatial uniformity has been particularly relevant in biological science where it is motivated, as Turing's original work was, by the challenge of understanding the origin of structure in embryology and related areas of development. Classic textbook surveys of pattern formation from various perspectives include [2–5].

On the mathematical side, much of this work has made use of a relatively small number of model equations which have attained a canonical status in the field; for example the Gierer–Meinhardt [6], Brusselator [7], Schnakenberg [8], and Gray-Scott [9] models of reaction–diffusion dynamics. It is noteworthy that the latter three of these models all contain cubic-order reaction terms, which would most parsimoniously be interpreted as describing the simultaneous interaction of three particles, despite this being intrinsically extremely unlikely and non-generic in a physical sense; alternatively one could consider this as a limiting case of a more complicated reaction scheme in which two particles form a complex which then rapidly interacts with a third particle. To the authors' knowledge, there are two published models of Turing instability with a mass-action reaction scheme having only quadratic nonlinearities: the Levin-Segel model for spatial pattern formation in phytoplankton distribution [10], and more recently from Woolley, Krause, and Gaffney, one of a pair of mass-action reaction diffusion PDEs which can be used to generate patterns in specific subregions of space [11]. Other models for spatial pattern formation, particularly those motivated by biological phenomena, employ a wide range of other forms of nonlinearity in the reaction–diffusion scheme, for example rational nonlinear functions (sigmoidal, Hill-type, Michaelis–Menten, etc.), which are also justifiable in terms of the equilibration on faster time scales of a subset of reaction processes,

* Corresponding author at: Department of Mathematical Sciences, University of Bath, Claverton Down, BA2 7AY, UK.
E-mail address: frw22@bath.ac.uk (F.R. Waters).

https://doi.org/10.1016/j.physd.2024.134427
Received 18 June 2024; Received in revised form 28 September 2024; Accepted 4 November 2024
Available online 19 November 2024

leaving the model describing the effective nature of the interactions on a slower timescale.

Our work focuses on the exploration and analysis of the simplest possible reaction schemes that contain only generic interaction terms, i.e those that contain only zeroth, first and second order reactions that correspond in mean-field PDE models to constant, linear, and quadratic terms, respectively. We then look for mean-field PDEs that are able to give rise to spatial patterns from an initially spatially homogeneous stable equilibrium state. In previous work [12] we established that quadratic polynomial reaction terms between two species, labelled U and V, with no separation of time scales and Fickian diffusion, can be sufficient for a homogeneous steady state to exist and to satisfy the conditions required for a linear instability with a preferred wavenumber that is positive, i.e. a 'Turing instability'. Such reaction dynamics are readily interpretable as arising from elementary reactions (i.e. reactions between at most two particles) under the assumption of mass-action kinetics. They therefore form a class of minimal reaction schemes through which we can directly link microscopic particle interactions to macroscopic Turing instability.

In [12], we computed the complete set of two-species mass-action reaction schemes that can exhibit Turing instability and which use the smallest possible number of elementary reactions. This analysis revealed that there was a fundamental difference between reaction schemes which could generate patterns in which the concentrations of the two chemical species fluctuated spatially in phase with each other (type-I) and those in which the two concentrations were spatially in antiphase (type-II). Minimal reaction schemes for type-I patterns contain only three reactions, whereas minimal reaction schemes for type-II patterns necessarily contain four reactions; it is not possible to generate type-II patterns with only three reactions. This work concentrated on the linear stability of spatially uniform equilibrium states and computed the conditions under which that state would become linearly unstable.

In this paper we develop this analysis further by considering the weakly nonlinear development of the linear instabilities previously identified. To be precise, we present here a complete analysis of the weakly nonlinear development of Turing instabilities for the type-I minimal reaction schemes, in one spatial dimension. Each scheme comprises a bi-particulate autocatalytic reaction of one species, $2U \to \ldots$, an inter-specific reaction $U+V \to \ldots$ which reduces the count of one or both species, and some third reaction. This third reaction, and the qualitative effects of the first two reactions on each species are what distinguish the different classes.

Although the weakly nonlinear asymptotic approach that we use is well-known, the results contain surprises and, as with many nonlinear analyses, would be extremely hard to predict without working through the details. Our analysis is partly analogous to that of Rottschäffer and Doelman in [13] – if one sets their cubic coefficients (a and b) to 0 – where the same generic amplitude modulation equation, and the same degenerate vanishing of coefficients, are considered in regards pattern evolution as one approaches the degeneracy. Here, in contrast, our focus is on the connections between our underlying particle-based reaction schemes and the sign of the determining coefficient in the amplitude equation, as well as establishing that stable patterns do indeed exist for the minimal models discussed here.

Our major conclusion is that we are able to show that all of these type-I reaction schemes, under certain conditions, are able to support stable, spatially periodic patterns that arise from the Turing instability: i.e. that for each type-I reaction scheme there exists an open region in parameter space, in which the instability will result in a stable patterned state that lies close to the species concentrations attained in the spatially uniform equilibrium. As a result, this analysis confirms that our set of type-I 'minimal schemes' are, with appropriate choices of parameter values, suitable models for the study of pattern formation, and can be connected directly to physically-realistic individual-based chemical reaction schemes.

Although it is difficult to summarise the results for all 11 classes of type-I together, our results allow a number of interesting conclusions to be drawn. First, we find that two cases, labelled in [12] as **c** and **d**, are unexpectedly degenerate in their nonlinear behaviour. We comment on these in great detail below, in Section 4 in particular. Turning to the other nine classes, a general conclusion is that the pattern forming instability is supercritical if the (pseudo-)reaction $2U \to n_1 U + m_1 V$ produces a sufficiently large number of particles of U compared to the number of particles of V that are produced, i.e. n_1 is sufficiently large compared to m_1. We make this statement precise in each subsection of Section 3 and express it in terms of the ratio of stoichiometric coefficients $\omega_1 := m_1/(n_1 - 2)$. In some classes the conditions for supercriticality involve a second stoichiometric ratio, denoted ω_3 which we define in the relevant subsections below. In these classes we find that it is always the case that for any fixed value of ω_3, the instability is supercritical for sufficiently small ω_1.

Finally, in cases in which the nature of the instability is not determined as expected at third order, more complicated analyses suggest that the reaction schemes are still able to sustain stable periodic patterns near the onset of the instability.

The remainder of the paper is organised as follows. Section 1 sets up the general structure of the PDE model that we analyse; i.e. a two species reaction–diffusion system with 'full' quadratic reaction terms, for which Turing instability occurs for appropriately chosen parameter values.

Section 2 presents the generic weakly nonlinear analysis for the problem. This multiple-scales analysis follows a standard route (see e.g. the textbook by Hoyle [3], or the review by Cross and Hohenberg [14]) and results, as expected, in a real Ginzburg–Landau equation [15,16], or, if we ignore the possibility of modulational dependence on a long spatial scale, a real Stuart–Landau equation [17,18]. The weakly nonlinear analysis therefore suggests that branches of steady patterned states bifurcate away from the zero amplitude solution as the ratio of diffusivities is varied. The character of this bifurcation is determined by the sign of the coefficient, $-K$, of the cubic term in the normal form, which we can determine explicitly but is a notably complicated function of the system parameters. General forms for the coefficients in the Ginzburg–Landau equation are well known: see [19] or [20] for general symbolic expressions, or [21] and more recently [22] which include code to compute them via symbolic manipulation. Here our focus is on finding the parameter regimes for which K is positive or negative.

In Section 3, we explore the general conditions for $K > 0$, corresponding to the case in which the pattern-forming instability is supercritical. Working through the 11 distinct classes of type-I minimal schemes, it is intriguing that the sign of K is fixed for any fixed choice of stoichiometry and does not depend on the reaction rates. In two classes (labelled **c** and **d**) we find, curiously, that K vanishes identically, for all choices of the stoichiometry, due to a particular orthogonality relation.

In Section 4 we investigate and resolve the behaviour in classes **c** and **d**, by using a different scaling for the leading order amplitude and applying the orthogonality condition to derive a cubic-quintic Ginzburg–Landau evolution equation. This prompts a more general form for the calculation (summarised in Section 5) of what happens when K vanishes. This exploration applies to the six classes in which K can take either sign, along codimension-two curves that form the boundary between regions of $K > 0$ and $K < 0$.

Together, the bifurcation behaviour predicted by the three subtly different amplitude equations in Sections 3–5 elucidates the picture of the weakly nonlinear behaviour of a general quadratic reaction model for Turing instability, and interprets this fully for the 11 cases of type-I instability. Specifically, we can evaluate when the appropriate coefficients are positive or negative, thus characterising the bifurcations as supercritical or subcritical, and, where they are supercritical we can quantitatively predict the pattern amplitude. These quantitative predictions are supported by numerical simulations, presented in Section 6. We summarise and draw conclusions in Section 7.

1. Problem specification

Under the usual assumptions of Fickian diffusion and mass-action reaction kinetics, the general PDE system for a reaction–diffusion system is

$$\begin{pmatrix} u_t \\ v_t \end{pmatrix} = \begin{pmatrix} D_1 & 0 \\ 0 & D_2 \end{pmatrix} \nabla^2 \begin{pmatrix} u \\ v \end{pmatrix} + \begin{pmatrix} F(u,v) \\ G(u,v) \end{pmatrix} , \tag{1}$$

where $u(\boldsymbol{x},t), v(\boldsymbol{x},t)$ are the concentrations of two species, $D_1, D_2 > 0$ are the species' diffusivities, F and G are, for the reasons outlined above, restricted to be quadratic polynomials, and the subscript t denotes the partial derivative with respect to t. We suppose that Eq. (1) supports a spatially uniform steady state (u^*, v^*). Rearranging about this state yields

$$\begin{pmatrix} u_t \\ v_t \end{pmatrix} = \left\{ \begin{pmatrix} D_1 & 0 \\ 0 & D_2 \end{pmatrix} \nabla^2 + J^* \right\} \begin{pmatrix} u-u^* \\ v-v^* \end{pmatrix} + N^* \begin{pmatrix} \frac{1}{2}(u-u^*)^2 \\ (u-u^*)(v-v^*) \\ \frac{1}{2}(v-v^*)^2 \end{pmatrix} ,$$

with

$$J^* := \begin{pmatrix} F^*_u & F^*_v \\ G^*_u & G^*_v \end{pmatrix} ,$$

$$N^* := \begin{pmatrix} F^*_{uu} & F^*_{uv} & F^*_{vv} \\ G^*_{uu} & G^*_{uv} & G^*_{vv} \end{pmatrix} ,$$

where subscripts $\cdot_u$, $\cdot_v$ denote partial derivatives with respect to u and v, respectively, and the superscript $\cdot^*$ denotes that these derivatives are evaluated at the steady state (u^*, v^*). We further assume that the steady state is Turing unstable – i.e. that it is linearly stable to spatially uniform perturbation, but is unstable to some spatially periodic perturbation with non-zero wavenumber. This enforces (by swapping species labels $u \leftrightarrow v$ if necessary) that the signs of the entries in the Jacobian J^* are

$$J^* \sim \begin{pmatrix} + & \mp \\ \pm & - \end{pmatrix} ,$$

that is: $J^*_{11} > 0 > J^*_{22}$ and $J^*_{12}J^*_{21} < 0$. By nondimensionalising $\hat{t} = J^*_{11}t$, $\hat{\boldsymbol{x}} = \sqrt{J^*_{11}/D_1}\boldsymbol{x}$ and defining $u - u^* = U$, $v - v^* = \sqrt{-J^*_{21}/J^*_{12}}V$, we obtain the following coupled PDEs for the (scaled) perturbations (U, V) to the homogeneous steady state:

$$\begin{pmatrix} U_{\hat{t}} \\ V_{\hat{t}} \end{pmatrix} = \left\{ \begin{pmatrix} 1 & 0 \\ 0 & \delta \end{pmatrix} \hat{\nabla}^2 + \begin{pmatrix} 1 & -\mu \\ \mu & -\vartheta \end{pmatrix} \right\} \begin{pmatrix} U \\ V \end{pmatrix} + \hat{N} \begin{pmatrix} \frac{1}{2}U^2 \\ UV \\ \frac{1}{2}V^2 \end{pmatrix} , \tag{2}$$

where

$$\delta := \frac{D_2}{D_1} , \quad \mu := -\sqrt{\frac{-J^*_{21}}{J^*_{12}}}\frac{J^*_{12}}{J^*_{11}} , \quad \vartheta := -\frac{J^*_{22}}{J^*_{11}} ,$$

$$\hat{N} := \frac{1}{J^*_{11}} \begin{pmatrix} 1 & 0 \\ 0 & \sqrt{-J^*_{12}/J^*_{21}} \end{pmatrix} \begin{pmatrix} F^*_{UU} & F^*_{UV} & F^*_{VV} \\ G^*_{UU} & G^*_{UV} & G^*_{VV} \end{pmatrix}$$

and $\partial_{\hat{t}}$ and $\hat{\nabla}$ denote, respectively, time and space derivatives with respect to $\hat{t}$ and $\hat{\boldsymbol{x}}$. From our assumption on the signs of the entries of the Jacobian J^*, we see that ϑ is necessarily positive. We observe that the sign of μ corresponds to the type of Turing instability the system may undergo: if $\mu > 0$ then concentration maxima of one species coincide with those of the other species, sometimes referred to as 'pure' activator-inhibitor dynamics — we refer to reaction schemes which exhibit these dynamics as 'type-I'. If $\mu < 0$, then concentration maxima of one species coincide with minima of the other species, often referred to as 'cross' activator-inhibitor dynamics; we refer to reaction schemes which exhibit these dynamics as 'type-II'. We analyse this governing PDE system (2) for U, V in one spatial dimension, so $\nabla^2 \equiv \partial^2_{xx}$, and we drop the hats $\hat{\cdot}$ for notational convenience.

1.1. Linearised analysis

Neglecting the nonlinear terms in Eq. (2), by the Routh–Hurwitz stability criteria, the uniform steady state $U = V = 0$ is linearly stable to spatially-independent perturbations if and only if

$$\vartheta > 1 \quad \text{and} \quad \mu^2 > \vartheta . \tag{3}$$

We shall assume that μ, ϑ are constrained so that inequalities (3) hold. Making the usual Fourier mode ansatz $(U, V) \propto \exp(\lambda t + ikx)$, under the linearisation we obtain

$$\left\{ -k^2 \begin{pmatrix} 1 & 0 \\ 0 & \delta \end{pmatrix} + \begin{pmatrix} 1 & -\mu \\ \mu & -\vartheta \end{pmatrix} - \lambda I \right\} \begin{pmatrix} U \\ V \end{pmatrix} = \mathbf{0} .$$

Equating the determinant of the matrix here to zero, we deduce the dispersion relation for $\lambda(k^2)$:

$$\lambda^2 + ((1+\delta)k^2 - (1-\vartheta))\lambda + (\delta k^4 - (\delta - \vartheta)k^2 + \mu^2 - \vartheta) = 0 . \tag{4}$$

After solving for λ, we find that the linearised temporal growth rate $\mathrm{Re}(\lambda(k^2))$ for a given wave number k is positive if and only if

$$\delta k^4 - (\delta - \vartheta)k^2 + \mu^2 - \vartheta < 0 . \tag{5}$$

From the constraint (3) that $\mu^2 > \vartheta$, there exist values of k that satisfy inequality (5) if and only if

$$\delta > \vartheta \quad \text{and} \quad (\delta - \vartheta)^2 > 4\delta(\mu^2 - \vartheta) ,$$

which, after some algebra, are satisfied simultaneously for some δ if and only if $\delta > \delta_0$ where

$$\delta_0 := \left(|\mu| + \sqrt{\mu^2 - \vartheta} \right)^2 .$$

Neglecting any selection mechanism on feasible perturbation modes (e.g. from boundary conditions), for example by assuming we are looking for solutions on an unbounded domain, the 'critical' wavenumber k_c – corresponding to the first unstable wavemode as δ increases past δ_0 – is therefore given by

$$k_c^2 = \frac{\delta_0 - \vartheta}{2\delta_0} , \tag{6}$$

and has linearised growth rate

$$\lambda(k_c^2) = \frac{k_c^2}{\delta_0 - 1}(\delta - \delta_0) + \mathcal{O}((\delta - \delta_0)^2) . \tag{7}$$

If $\delta > \delta_0$, then the interval (k_-, k_+) of wavenumbers for which the growth rate λ is positive is defined by

$$k_\pm := k_c \pm \left(\frac{1 - k_c^2}{4\delta_0} \right)^{\frac{1}{2}} (\delta - \delta_0)^{\frac{1}{2}} + \mathcal{O}(\delta - \delta_0) . \tag{8}$$

Thus, as we expect for steady-state pattern formation problems where the dispersion relation has a locally quadratic maximum, if $\delta - \delta_0 = \mathcal{O}(\varepsilon^2)$ where $\varepsilon > 0$ is small, then the characteristic growth rate of the critical instability mode is $\mathcal{O}(\varepsilon^2)$, while the width of the band of unstable wavenumbers is $\mathcal{O}(\varepsilon)$.

2. Weakly nonlinear analysis

To explore the weakly nonlinear behaviour of the system close to the Turing instability threshold, we let $\delta = \delta_0 + \delta_2\varepsilon^2$ for some small parameter $\varepsilon > 0$. In line with the scalings noted at the end of the previous section, we anticipate that the generic weakly nonlinear dynamics will evolve on the slow time scale $T = \varepsilon^2 t$, and long length scale $X = \varepsilon x$. We consider T and X to be formally independent of t and x, and look for solutions $U(x, X, T)$, $V(x, X, T)$ to the governing Eq. (2) that are independent of the fast time scale t, since the linear instability does not exhibit rapid oscillations in time. Thus we rewrite $\partial_t \mapsto \varepsilon^2\partial_T$, $\partial_x \mapsto \partial_x + \varepsilon\partial_X$. Substituting these scalings into the governing PDEs we obtain

$$\varepsilon^2 \begin{pmatrix} U_T \\ V_T \end{pmatrix} = \mathcal{L} \begin{pmatrix} U \\ V \end{pmatrix} + (2\varepsilon\partial_{xX} + \varepsilon^2\partial_{XX}) \begin{pmatrix} U \\ \delta_0 V \end{pmatrix}$$

$$+\varepsilon^2(\partial_{xx}+2\varepsilon\partial_{xX}+\varepsilon^2\partial_{XX})\begin{pmatrix}0\\ \delta_2 V\end{pmatrix}+N\begin{pmatrix}\frac{1}{2}U^2\\ UV\\ \frac{1}{2}V^2\end{pmatrix}, \tag{9}$$

where

$$\mathcal{L}:=\begin{pmatrix}1 & 0\\ 0 & \delta_0\end{pmatrix}\partial_{xx}+\begin{pmatrix}1 & -\mu\\ \mu & -\vartheta\end{pmatrix}$$

is the $\mathcal{O}(1)$ part of the linear operator. It is useful to define

$$L_p:=-p^2k_c^2\begin{pmatrix}1 & 0\\ 0 & \delta_0\end{pmatrix}+\begin{pmatrix}1 & -\mu\\ \mu & -\vartheta\end{pmatrix},\ p\geqslant 0,$$

which describes the action of $\mathcal{L}$ on a pair of functions (f_1,f_2) that have short length scale dependence $f_j(x)\propto\exp(\pm ipk_cx)$.

Using the relations (5) and (6) we deduce the useful result that $\mu^2-\vartheta=\delta_0k_c^4$ from which we can deduce, via a direct calculation, that $\det(L_p)=(p^2-1)^2\delta_0k_c^4$, and so L_p is invertible if and only if $p\neq 1$. We now propose an asymptotic expansion

$$\begin{pmatrix}U\\ V\end{pmatrix}=\varepsilon\begin{pmatrix}U_1\\ V_1\end{pmatrix}+\varepsilon^2\begin{pmatrix}U_2\\ V_2\end{pmatrix}+\varepsilon^3\begin{pmatrix}U_3\\ V_3\end{pmatrix}+\cdots,$$

and solve Eq. (9) for the amplitudes (U_j,V_j) order-by-order.

2.1. Solution at order ε

At leading order, we recover the linear problem:

$$\mathbf{0}=\mathcal{L}\begin{pmatrix}U_1\\ V_1\end{pmatrix},$$

and for a non-zero leading order solution, we deduce that (U_1,V_1) must have short length scale dependence $\exp(\pm ik_cx)$, such that it lies in the kernel of $\mathcal{L}$. Thus we have an eigenvector problem

$$L_1\begin{pmatrix}U_1\\ V_1\end{pmatrix}=\mathbf{0}\implies\begin{pmatrix}U_1\\ V_1\end{pmatrix}=(a+\bar{a})\boldsymbol{\eta}, \tag{10}$$

where $\boldsymbol{\eta}$ is the right-eigenvector of L_1 with eigenvalue 0:

$$\boldsymbol{\eta}:=\begin{pmatrix}-\mu\\ -(1-k_c^2)\end{pmatrix},$$

and $a(x,X,T)=\exp(ik_cx)A(X,T)$ where $A(X,T)$ is a complex-valued amplitude. We use overbars $\bar{\cdot}$ to denote complex conjugate. We also define $\boldsymbol{\xi}$ to be the left-eigenvector of L_1 with eigenvalue 0:

$$\boldsymbol{\xi}:=\begin{pmatrix}\mu\\ -(1-k_c^2)\end{pmatrix},$$

and we note, intriguingly that $\boldsymbol{\xi}^\intercal$ and $\boldsymbol{\eta}$ satisfy conditions involving, separately, the diffusion and reaction terms:

$$\boldsymbol{\xi}^\intercal\begin{pmatrix}1 & 0\\ 0 & \delta_0\end{pmatrix}\boldsymbol{\eta}=\boldsymbol{\xi}^\intercal\begin{pmatrix}1 & -\mu\\ \mu & -\vartheta\end{pmatrix}\boldsymbol{\eta}=0. \tag{11}$$

This in itself is curious, though it appears generic to any Turing instability in a system with Fickian or 'diagonal' diffusion: the right- and left-eigenvectors of L_1 with eigenvalue zero together annihilate both the steady state Jacobian and separately the diffusion matrix at criticality.

2.2. Solution at order ε^2

Retaining only the next-to-leading order terms from Eq. (9), and substituting in the leading-order solution (10), we find

$$\mathcal{L}\begin{pmatrix}U_2\\ V_2\end{pmatrix}=-2ik_c(a_X-\bar{a}_X)\begin{pmatrix}1 & 0\\ 0 & \delta_0\end{pmatrix}\boldsymbol{\eta}-\left(|a|^2+\frac{1}{2}(a^2+\bar{a}^2)\right)M\boldsymbol{\eta}, \tag{12}$$

where the 2×2 matrix M is most compactly written as the product of the 2×3 matrix N of coefficients of the nonlinear terms and a 3×2 matrix:

$$M:=N\begin{pmatrix}-\mu & 0\\ -(1-k_c^2) & -\mu\\ 0 & -(1-k_c^2)\end{pmatrix}. \tag{13}$$

Given the x-dependencies on the right-hand side of Eq. (12), we look for a solution

$$\begin{pmatrix}U_2\\ V_2\end{pmatrix}=\boldsymbol{w}^{(0)}+\boldsymbol{w}^{(1)}+\boldsymbol{w}^{(2)},$$

where $\boldsymbol{w}^{(p)}$ contains only terms with short length-scale dependencies $\exp(\pm ipk_cx)$. The linearity of $\mathcal{L}$ then implies that (12) decomposes into three uncoupled equations:

$$L_0\boldsymbol{w}^{(0)}=-|a|^2M\boldsymbol{\eta},$$

$$L_1\boldsymbol{w}^{(1)}=-2ik_c\begin{pmatrix}1 & 0\\ 0 & \delta_0\end{pmatrix}(a_X-\bar{a}_X)\boldsymbol{\eta},$$

$$L_2\boldsymbol{w}^{(2)}=-\frac{1}{2}(a^2+\bar{a}^2)M\boldsymbol{\eta}.$$

The solution components $\boldsymbol{w}^{(0)},\boldsymbol{w}^{(2)}$ are determined uniquely since L_0 and L_2 are invertible. In addition, the middle equation, for $\boldsymbol{w}^{(1)}$, is also soluble, as the right-hand side lies in the image space of L_1. In this case $\boldsymbol{w}^{(1)}$ is determined only up to an additive scalar multiple of $\boldsymbol{\eta}$. No extra information about the nonlinear behaviour is gained by including this homogeneous component (being effectively a copy of the leading order solution but shifted down an order of ε), so we choose $\boldsymbol{w}^{(1)}$ to be orthogonal to $\boldsymbol{\eta}$. Defining

$$\boldsymbol{\zeta}:=\frac{-\delta_0}{(\delta_0+1)\mu}\begin{pmatrix}1-k_c^2\\ -\mu\end{pmatrix},$$

which satisfies

$$L_1\boldsymbol{\zeta}=\begin{pmatrix}1 & 0\\ 0 & \delta_0\end{pmatrix}\boldsymbol{\eta},$$

we find the solution:

$$\begin{pmatrix}U_2\\ V_2\end{pmatrix}=-2ik_c(a_X-\bar{a}_X)\boldsymbol{\zeta}-|a|^2L_0^{-1}M\boldsymbol{\eta}-\frac{1}{2}(a^2+\bar{a}^2)L_2^{-1}M\boldsymbol{\eta}, \tag{14}$$

where we have not evaluated fully the vectors $L_0^{-1}M\boldsymbol{\eta}$ and $L_2^{-1}M\boldsymbol{\eta}$ since this is, in general, just algebraically lengthy.

2.3. Solution at order ε^3

At the next order, we obtain terms with a long time derivative ∂_T, and we may obtain an evolution equation for the amplitude $A(X,T)$. Retaining terms of order ε^3 from the governing Eq. (9) and substituting in the leading order solution (10), we find

$$\mathcal{L}\begin{pmatrix}U_3\\ V_3\end{pmatrix}=(a_T+\bar{a}_T)\boldsymbol{\eta}-(a_{XX}+\bar{a}_{XX})\begin{pmatrix}1 & 0\\ 0 & \delta_0\end{pmatrix}\boldsymbol{\eta}$$
$$-k_c^2(1-k_c^2)(a+\bar{a})\begin{pmatrix}0\\ \delta_2\end{pmatrix}-2\partial_{xX}\begin{pmatrix}U_2\\ \delta_0V_2\end{pmatrix}-(a+\bar{a})M\begin{pmatrix}U_2\\ V_2\end{pmatrix}.$$

In order for this to be solvable for (U_3,V_3), all terms on the right-hand side with x-dependency $\exp(\pm ik_cx)$ must lie in the image space of L_1 – i.e. orthogonal to $\boldsymbol{\xi}$. Substituting in for (U_2,V_2) using (14) and taking an inner product with $\boldsymbol{\xi}^\intercal$, we obtain the solvability condition

$$\frac{\delta_0-1}{k_c^2}A_T=\frac{4\delta_0}{1-k_c^2}A_{XX}+\delta_2A-\frac{K}{k_c^2(1-k_c^2)^2}A|A|^2. \tag{15}$$

where the coefficient K is defined to be

$$K:=-\boldsymbol{\xi}^\intercal M\left(L_0^{-1}+\tfrac{1}{2}L_2^{-1}\right)M\boldsymbol{\eta}.$$

Scaling our variables

$$T=\frac{\delta_0-1}{k_c^2}\hat{T},\ X=\left(\frac{4\delta_0}{1-k_c^2}\right)^{\frac{1}{2}}\hat{X},\ A=k_c(1-k_c^2)\hat{A},$$

and neglecting the hats, we obtain the real Ginzburg–Landau equation

$$A_T=A_{XX}+\delta_2A-KA|A|^2. \tag{16}$$

If A is independent of the long-lengthscale X, this reduces to the Stuart–Landau equation

$$A_T=\delta_2A-KA|A|^2.$$

The characteristic T- and X-scalings deployed to obtain Eq. (16) are as expected from the asymptotic expansions (7) and (8) respectively, while the scaling for A ensures that the cubic term balances the terms with derivatives.

If $K > 0$, then stable stripe pattern solutions with $|A| = (\delta_2/K)^{1/2}$ are expected to bifurcate from the linearly unstable zero amplitude solution for $\delta_2 > 0$ (the Turing instability regime), while if $K < 0$ then linearly unstable stripe patterns bifurcate away from the linearly stable zero solution and exist in the region $\delta_2 < 0$ (i.e. outside the region of parameter space where the uniform state is Turing-unstable). In the latter, 'subcritical', case, it is possible that the branches of patterned solutions will turn around in parameter space, through saddle–node bifurcations, resulting in stable patterned states that exist on both sides of the bifurcation point. For any given reaction scheme, it is therefore essential to understand the sign of K.

3. The sign of K

After some algebraic rearrangement, presented in detail in Appendix A, we can write K as

$$K = -\frac{5}{6}\frac{\boldsymbol{\xi}^\intercal M\boldsymbol{\eta}}{\delta_0 k_c^2}\left(\frac{19}{15}\frac{\boldsymbol{\xi}^\intercal M\boldsymbol{\eta}}{k_c^2(1-k_c^2)} + \delta_0 M_{11} + M_{22}\right), \tag{17}$$

where M_{ij} denotes the (i,j)th entry of the matrix M. Thus K is positive if (and only if) either

$$\delta_0 M_{11} + M_{22} > -\frac{19}{15}\frac{\boldsymbol{\xi}^\intercal M\boldsymbol{\eta}}{k_c^2(1-k_c^2)} > 0 \tag{18a}$$

$$\text{or } \delta_0 M_{11} + M_{22} < -\frac{19}{15}\frac{\boldsymbol{\xi}^\intercal M\boldsymbol{\eta}}{k_c^2(1-k_c^2)} < 0\,, \tag{18b}$$

and we note that K can vanish if (and only if) either

$$\boldsymbol{\xi}^\intercal M\boldsymbol{\eta} = 0$$

$$\text{or } \boldsymbol{\xi}^\intercal M\boldsymbol{\eta} = -\frac{15}{19}k_c^2(1-k_c^2)\left(\delta_0 M_{11} + M_{22}\right)\,.$$

In our previous work [12], we derived a complete classification of minimal mass-action reaction schemes, involving only elementary reactions (i.e. where reactions may occur between at most two particles), that can exhibit Turing instability. This previous work focused on the derivation of the classification itself through the linear analysis that determines when a Turing instability is possible. Now, having presented the weakly nonlinear analysis in Section 2, and using the inequalities (18a) and (18b), we can explore directly the weakly nonlinear development of the Turing instability. That is, in terms of stoichiometric coefficients and reaction rate parameters, we can derive the conditions under which these minimal schemes may be expected to support stable patterned solutions, at least in the vicinity of the Turing instability threshold at $\delta = \delta_0$.

For our minimal type-I schemes (those for which the concentrations spatially oscillate in-phase, also referred to as a pure-Turing instability as opposed to cross-activator-inhibitor dynamics), it turns out that sign(K) is independent of the values of the reaction rate parameters. As discussed in the introduction, we focus our attention here on these classes of minimal scheme and in later subsections present details of all 11 minimal type-I classes. The results are summarised in Figs. 1 and 2 which show, for each type-I class, a plot illustrating sign(K) as a function of either one ratio, which we denote by ω_1, or two ratios (denoted by ω_1 and ω_3) of the stoichiometric effects of the underlying reactions.

For each class we can show that inequality (18b) is the relevant condition determining the sign of K, i.e. $\delta_0 M_{11} + M_{22} < 0 < \boldsymbol{\xi}^\intercal M\boldsymbol{\eta}$ for all choices of stoichiometry which permit Turing instability, and thus K is positive if and only if inequality (18b) holds.

Intriguingly we find that for classes **c** and **d** it is the case that $\boldsymbol{\xi}^\intercal M\boldsymbol{\eta} = 0$ for any choice of reaction stoichiometry and rate parameters such that Turing instability occurs, and so $K \equiv 0$. This is due to a particular degeneracy of the nonlinear terms and is explored in detail in Section 3.2. This then motivates additional weakly nonlinear analysis which we present in Section 4. All the other classes contain Turing-unstable reaction schemes for which $K > 0$, and some contain Turing-unstable reaction schemes for which $K < 0$. Where there is a boundary $K = 0$, we see that K is positive for sufficiently small ω_1, below a threshold value which may depend on the other ratio ω_3.

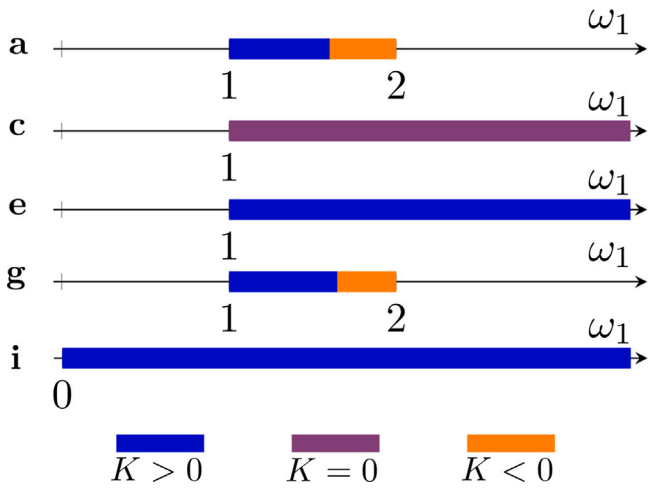

Fig. 1. Graphical illustration of the sign of K for five of the 11 classes of minimal type-I Turing-unstable reaction schemes. Letters **a**, **c**, **e**, **g**, **i** denote the different minimal schemes labelled as in [12] and as set out in the separate subsections of Section 3. In each case, within the Turing unstable regime, sign(K) is a function of only a single parameter: $\omega_1 = m_1/(n_1 - 2)$, the ratio of the stoichiometric effects on the second and first species due to the (pseudo-)reaction $2U \to n_1 U + m_1 V$. In **a** and **g**, at the boundary between $K > 0$ and $K < 0$ there is a unique value for ω_1 which yields $K = 0$. Also in **a** and **g**, there are upper and lower bounds on ω_1 beyond which a Turing instability does not occur; in **c**, **e** and **i** there is only a lower bound on ω_1.

To reduce the amount of analysis required, we group the 11 schemes into five pairs and one singleton. In each case, subject to the stoichiometric conditions that permit Turing instability — which we simply state here, but are derived in detail in [12] – the nondimensionalised form, Eq. (2), is derived explicitly, and we then show that either

(i): $\delta_0 M_{11} + M_{22} < 0$ and $\boldsymbol{\xi}^\intercal M\boldsymbol{\eta} > 0$, or

(ii): $\boldsymbol{\xi}^\intercal M\boldsymbol{\eta} = 0$.

The two classes that satisfy this second condition (**c** and **d**) are the subject of the analysis in Section 3.2; for the rest, given the stoichiometric conditions for the reaction scheme to be Turing-unstable, K is positive if and only if inequality (18b) is satisfied:

$$\frac{19}{15}\frac{\boldsymbol{\xi}^\intercal M\boldsymbol{\eta}}{k_c^2(1-k_c^2)} < -(\delta_0 M_{11} + M_{22})\,.$$

In all cases this can be simplified to an inequality involving only ratios of the stoichiometric effects of each reaction on each species. What we mean by this is that for a Turing-unstable reaction scheme of three reactions:

$$\begin{cases} p_1 U + q_1 V \xrightarrow{r_1} n_1 U + m_1 V \\ p_2 U + q_2 V \xrightarrow{r_2} n_2 U + m_2 V \\ p_3 U + q_3 V \xrightarrow{r_3} n_3 U + m_3 V \end{cases}$$

the sign of K depends only on the ratios

$$(n_i - p_i) : (m_i - q_i),\ i = 1, 2, 3\,.$$

To this end, we will express the results in terms of the variables $\omega_i = |m_i - q_i|/|n_i - p_i|$ and $\varpi_i = |n_i - p_i|/|m_i - q_i|$ (to avoid dividing by zero) as appropriate. It is important to note in the presentation of different classes that the definitions of the ω_i and ϖ_i may differ from one class

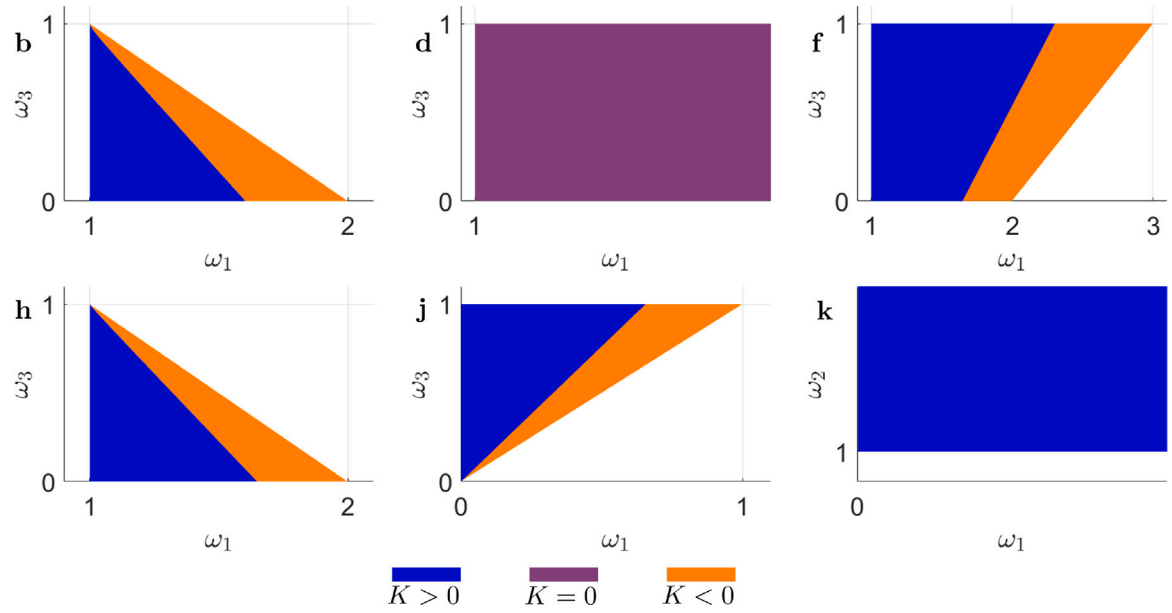

Fig. 2. Sign of K for the remaining six classes of minimal type-I Turing-unstable reaction schemes. In each of these, within the Turing unstable regime, sign(K) is a function of two ratios (as opposed to one, for the classes in Fig. 1) of stoichiometric effects. Letters **b**, **d**, **f**, **h**, **j** and **k** correspond to the classification of minimal schemes as in [12]. White regions do not allow a Turing instability to take place; the boundaries of the coloured regions are set out in the relevant sub-sections of Section 3.

to another, although in classes **a**, **c**, **e**, **g** and **i** we consistently define $\omega_1 = m_1/(n_1-2)$ which is the ratio of the stoichiometric increases in the second and first species, respectively, in the reaction $2U \to n_1 U + m_1 V$.

We summarise the results in Figs. 1 and 2. In classes **e**, **i** and **k** we find that K is sign definite. In other classes sign(K) is a particularly simple function of ω_i, in others we defer to numerical evaluation.

3.1. Classes **a** and **b**

Recalling essential details from [12], the reaction schemes for classes **a** and **b** and associated stoichiometric conditions to allow Turing instability are

$$\mathbf{a}\begin{cases} 2U & \xrightarrow{r_1} n_1'' U + m_1 V \\ U+V & \xrightarrow{r_2} \emptyset \\ \emptyset & \xrightarrow{r_3} n_3 U \end{cases}$$

subject to: $2(n_1''-2) > m_1 > n_1''-2$,

and

$$\mathbf{b}\begin{cases} 2U & \xrightarrow{r_1} n_1'' U + m_1 V \\ U+V & \xrightarrow{r_2} \emptyset \\ \emptyset & \xrightarrow{r_3} n_3 U + m_3 V \end{cases}$$

subject to: $2(n_1''-2)n_3 > m_1 n_3 + (n_1''-2)m_3$, $m_1 > n_1''-2$, $n_3 > m_3$,

where the reaction rate constants r_i are positive. We note that for all choices of the stoichiometry there is always a non-empty open subset of $\mathbb{R}^3_+$ in which the values of (r_1, r_2, r_3) enable a Turing instability to take place. The coefficients n_i, m_i of the reaction products are always nonnegative integers, and following the notation of [12]: primes are used to indicate additional imposed constraints, specifically that coefficients denoted by a single prime are greater than one, e.g. $n_i', m_i' > 1$ and double primes denote coefficients greater than two: $n_i'', m_i'' > 2$. The corresponding mean-field PDE model for the concentrations $u(\boldsymbol{x}, t)$ and $v(\boldsymbol{x}, t)$ is

$$u_t = D_u \nabla^2 u + \hat{r}_3 + \hat{r}_1 u^2 - r_2 uv \ ,$$
$$v_t = D_v \nabla^2 v + \hat{r}_3 \omega_3 + \hat{r}_1 \omega_1 u^2 - r_2 uv \ ,$$

where $\hat{r}_1 = (n_1''-2)r_1$, $\hat{r}_3 = n_3 r_3$, and we define the stoichiometric ratios

$$\omega_1 := \frac{m_1}{n_1''-2} \ , \quad \omega_3 := \frac{m_3}{n_3} \ .$$

For the reaction scheme to be Turing-unstable, we find that these must satisfy $0 \leqslant \omega_3 < 1$ and $1 < \omega_1 < 2 - \omega_3$. If $\omega_3 = 0$ then we are considering scheme **a**, otherwise we are considering scheme **b**. By rescaling $u = u^* + U$, $v = v^* + vV$, about the homogeneous steady state

$$u^* = \sqrt{\frac{\hat{r}_3}{\hat{r}_1}}\sqrt{\frac{1-\omega_3}{\omega_1-1}} \ , \quad v^* = \sqrt{\frac{\hat{r}_1\hat{r}_3}{r_2^2}}\frac{\omega_1-\omega_3}{\sqrt{(\omega_1-1)(1-\omega_3)}}$$

we transform the PDE model (1) into the nondimensionalised form

$$\begin{pmatrix} U_{\hat{t}} \\ V_{\hat{t}} \end{pmatrix} = \left\{ \begin{pmatrix} 1 & 0 \\ 0 & \delta \end{pmatrix} \hat{\nabla}^2 + \begin{pmatrix} 1 & -\mu \\ \mu & -\vartheta \end{pmatrix} \right\} \begin{pmatrix} U \\ V \end{pmatrix} + N \begin{pmatrix} \frac{1}{2}U^2 \\ UV \end{pmatrix} \ , \tag{19}$$

where $t = \tau\hat{t}$, $\boldsymbol{x} = \sqrt{\tau D_1}\hat{\boldsymbol{x}}$, and

$$\tau = \frac{1}{\sqrt{\hat{r}_1\hat{r}_3}}\frac{\sqrt{(\omega_1-1)(1-\omega_3)}}{2-\omega_1-\omega_3} \ ,$$
$$\nu = \frac{1}{\sqrt{\hat{\rho}}}\sqrt{2(\omega_1-1) + \frac{2-\omega_1-\omega_3}{1-\omega_3}} \ ,$$
$$\vartheta = \hat{\rho}\frac{1-\omega_3}{2-\omega_1-\omega_3} \ ,$$
$$\mu = \nu\vartheta \ ,$$
$$N = \hat{r}_1\tau \begin{pmatrix} 2 & -\hat{\rho}\nu \\ 2\omega_1\nu^{-1} & -\hat{\rho} \end{pmatrix} \ , \quad \hat{\rho} = \frac{r_2}{\hat{r}_1} \ .$$

We note that we have taken N to be a 2×2 matrix here since there are no V^2 terms in the PDE model; in the definition of N as a 2×3 matrix the entries N_{31}, N_{32} in the final column are (for these reaction schemes) both zero. In this section, we continue to omit these zero entries, since the lack of V^2 terms is common to all the minimal reaction schemes for type-I instability, as is the form of the nondimensionalisation (19); what varies between classes of schemes is how the coefficients $\tau, \nu, \vartheta, \mu, N$ depend on the system parameters. For classes **a** and **b**, we have that the matrix M defined in (13) takes the form

$$M = \frac{-\hat{r}_1\tau}{2\delta_0\vartheta}\begin{pmatrix} 4\delta_0\mu\vartheta - \hat{\rho}\mu(\delta_0+\vartheta) & -2\hat{\rho}\delta_0\mu^2 \\ 4\omega_1\delta_0\vartheta^2 - \hat{\rho}\vartheta(\delta_0+\vartheta) & -2\hat{\rho}\delta_0\mu\vartheta \end{pmatrix} \ ,$$

thus

$$\delta_0 M_{11} + M_{22} = \frac{-r_2\tau\mu[(\omega_1-1)(\delta_0+3\vartheta)+3(1-\omega_3)(\delta_0-\vartheta)]}{2\vartheta(2-\omega_1-\omega_3)} ,$$

which is always negative. A direct calculation finds that

$$\boldsymbol{\xi}^{\mathsf{T}} M \boldsymbol{\eta} = \hat{r}_1\tau\mu\frac{\delta_0+\vartheta}{4\delta_0^2}\left(\frac{4(\omega_1-1)(\omega_1-\omega_3)}{2-\omega_1-\omega_3}\delta_0\vartheta + \frac{\omega_1-1}{1-\omega_3}(\delta_0^2-\vartheta^2)\right) ,$$

which is always positive. Accordingly, after much rearranging we can deduce that, provided that ω_3 and/or ω_1 are chosen such that the reaction scheme is Turing-unstable, K is positive if and only if

$$(\omega_1-1)\big(8+273(1-\omega_3)\big) - 169\left(1-\omega_3\right)^2 < 0.$$

For class **a** we have $\omega_3 = 0$, so this condition then simplifies to become

$$K > 0 \iff \omega_1 < \frac{450}{281} \approx 1.6014 .$$

For class **b** the inequality involves both ω_1 and ω_3 and is represented graphically in the top-left panel of Fig. 2.

3.2. Classes **c** and **d**

The reaction schemes and associated stoichiometric conditions to allow Turing instability for classes **c** and **d** are

$$\mathbf{c}\ \begin{cases} 2U \xrightarrow{r_1} n_1''U + m_1V \\ U+V \xrightarrow{r_2} \emptyset \\ U \xrightarrow{r_3} n_3'U \end{cases}$$

subject to: $m_1 > n_1'' - 2$,

and

$$\mathbf{d}\ \begin{cases} 2U \xrightarrow{r_1} n_1''U + m_1V \\ U+V \xrightarrow{r_2} \emptyset \\ U \xrightarrow{r_3} n_3'U + m_3V \end{cases}$$

subject to: $m_1 > n_1'' - 2$, $n_3' - 1 > m_3$.

The corresponding mean-field PDE model is

$$u_t = D_u\nabla^2 u + \hat{r}_3 u + \hat{r}_1 u^2 - r_2 uv ,$$
$$v_t = D_v\nabla^2 v + \hat{r}_3\omega_3 u + \hat{r}_1\omega_1 u^2 - r_2 uv ,$$

where $\hat{r}_1 = (n_1''-2)r_1$, $\hat{r}_3 = (n_3'-1)r_3$,

$$\omega_1 := \frac{m_1}{n_1''-2} , \quad \omega_3 := \frac{m_3}{n_3'-1} ,$$

and for the reaction scheme to be Turing-unstable, these must satisfy $0 \leqslant \omega_3 < 1 < \omega_1$. Class **c** is defined by the special case of $\omega_3 = 0$; if $\omega_3 \neq 0$ then we are considering class **d**. As previously, by rescaling $u = u^* + U$, $v = v^* + vV$, about the homogeneous steady state

$$u^* = \frac{\hat{r}_3}{\hat{r}_1}\frac{1-\omega_3}{\omega_1-1} , \quad v^* = \frac{\hat{r}_3}{r_2}\frac{\omega_1-\omega_3}{\omega_1-1} ,$$

we are able to put this into the nondimensionalised form (19), where now

$$\tau = \frac{1}{\hat{r}_3}\frac{\omega_1-1}{1-\omega_3} ,$$
$$\nu = \frac{1}{\sqrt{\hat{\rho}}}\sqrt{\omega_1} ,$$
$$\vartheta = \hat{\rho} ,$$
$$\mu = \sqrt{\hat{\rho}}\sqrt{\omega_1} ,$$
$$N = \tau\hat{r}_1\begin{pmatrix} 2 & -\hat{\rho}\nu \\ 2\omega_1\nu^{-1} & -\hat{\rho}\end{pmatrix} , \quad \hat{\rho} = \frac{r_2}{\hat{r}_1} .$$

This gives that

$$M = -\frac{\tau\hat{r}_1}{2\delta_0}\begin{pmatrix} 3\delta_0\mu - \mu\vartheta & -2\delta_0\mu^2 \\ \delta_0(\delta_0+\vartheta) & -2\delta_0\mu\vartheta\end{pmatrix} \quad \text{and} \quad \boldsymbol{\xi}^{\mathsf{T}} M\boldsymbol{\eta} = 0 ,$$

and hence $K = 0$ for all combinations of parameters in these two cases. The explanation for this degeneracy can be seen clearly when we write the system out fully in its nondimensionalised form:

$$\begin{pmatrix} U_{\hat{t}} \\ V_{\hat{t}}\end{pmatrix} = \left\{\begin{pmatrix} 1 & 0 \\ 0 & \delta\end{pmatrix}\hat{\nabla}^2 + \begin{pmatrix} 1 & -\mu \\ \mu & -\vartheta\end{pmatrix}\right\}\begin{pmatrix} U \\ V\end{pmatrix} + \frac{1}{u^*}U\begin{pmatrix} 1 & -\mu \\ \mu & -\vartheta\end{pmatrix}\begin{pmatrix} U \\ V\end{pmatrix} .$$

Since all the reaction terms, in both equations, involve a factor of U, the coefficients in the quadratic terms are precisely the same as those in the linear terms. This does not, of course, depend on the nondimensionalisation itself and holds also in other statements of the problem, for example specialising the PDE system (1) to the form

$$\begin{pmatrix} u_t \\ v_t\end{pmatrix} = \begin{pmatrix} D_1 & 0 \\ 0 & D_2\end{pmatrix}\nabla^2\begin{pmatrix} u \\ v\end{pmatrix} + \begin{pmatrix} uf(u,v) \\ ug(u,v)\end{pmatrix} ,$$

in which all the nonlinear terms contain a factor of u and f and g have vanishing second partial derivatives at the (nonzero) steady state. When this holds, relations such as (11) emerge directly in the nonlinear parts of the calculations and result in the quantity $\boldsymbol{\xi}^{\mathsf{T}} M\boldsymbol{\eta}$ vanishing identically.

3.3. Classes **e** and **f**

For these two classes, the reaction schemes and stoichiometric conditions to allow Turing instability are

$$\mathbf{e}\ \begin{cases} 2U \xrightarrow{r_1} n_1''U + m_1V \\ U+V \xrightarrow{r_2} \emptyset \\ V \xrightarrow{r_3} \emptyset \end{cases}$$

subject to: $m_1 > n_1'' - 2$,

and

$$\mathbf{f}\ \begin{cases} 2U \xrightarrow{r_1} n_1''U + m_1V \\ U+V \xrightarrow{r_2} \emptyset \\ V \xrightarrow{r_3} n_3U \end{cases}$$

subject to: $m_1 > n_1'' - 2$, $(n_1''-2)(2n_3+1) > m_1 n_3$,

and the corresponding mean-field PDE model is

$$u_t = D_u\nabla^2 u + r_3\varpi_3 v + \hat{r}_1\varpi_1 u^2 - r_2 uv ,$$
$$v_t = D_v\nabla^2 v - r_3 v + \hat{r}_1 u^2 - r_2 uv ,$$

where $\hat{r}_1 = m_1 r_1$, and we define

$$\varpi_1 := \frac{n_1''-2}{m_1} , \quad \varpi_3 := n_3 .$$

For the reaction scheme to be Turing-unstable, ϖ_1 and ϖ_3 must satisfy $\varpi_3/(2\varpi_3+1) < \varpi_1 < 1$. Class **e** is the case $\varpi_3 = 0$, and class **f** is the case $\varpi_3 \neq 0$. Rescaling $u = u^* + U$, $v = v^* + \nu V$ about the homogeneous steady state

$$u^* = \frac{r_3}{r_2}\frac{\varpi_3+\varpi_1}{1-\varpi_1} , \quad v^* = \frac{\hat{r}_1 r_3}{r_2^2}\frac{(\varpi_3+\varpi_1)^2}{(1-\varpi_1)(\varpi_3+1)} ,$$

we obtain the nondimensionalised form (19) with

$$\tau = \frac{r_2}{\hat{r}_1 r_3}\frac{(1-\varpi_1)(\varpi_3+1)}{(\varpi_3+\varpi_1)((2\varpi_3+1)\varpi_1-\varpi_3)} ,$$
$$\nu = \frac{1}{\sqrt{\hat{\rho}}}\sqrt{\frac{(\varpi_3+\varpi_1)(\varpi_3+2-\varpi_1)}{(\varpi_3+1)^2\varpi_1}},$$
$$\vartheta = \hat{\rho}\frac{(\varpi_3+1)^2}{(\varpi_3+\varpi_1)((2\varpi_3+1)\varpi_1-\varpi_3)} ,$$
$$\mu = \nu\varpi_1\vartheta ,$$
$$\hat{N} = \tau\hat{r}_1\begin{pmatrix} 2\varpi_1 & -\hat{\rho}\nu \\ 2\nu^{-1} & -\hat{\rho}\end{pmatrix} , \quad \hat{\rho} = \frac{r_2}{\hat{r}_1} .$$

Direct calculation of the matrix M gives

$$M = -\frac{\tau\hat{r}_1}{2\delta_0}\begin{pmatrix} 4\varpi_1\delta_0\mu - \hat{\rho}\mu\frac{\delta_0+\vartheta}{\varpi_1\vartheta} & -2\hat{\rho}\delta_0\mu^2/(\varpi_1\vartheta) \\ 4\varpi_1\delta_0\vartheta - \hat{\rho}(\delta_0+\vartheta) & -2\hat{\rho}\delta_0\mu\end{pmatrix}$$

and so, after considerable algebra,

$$\delta_0 M_{11} + M_{22} = -\frac{\tau\hat{r}_1\mu}{2\varpi_1}\left(\left(\frac{\varpi_3^2(1-\varpi_1)^2}{(\varpi_3+1)^2} + 3\varpi_1^2\right)(\delta_0-\vartheta)\right.$$

$$+\frac{2(1-\varpi_1)}{(\varpi_3+1)^2}\left(\varpi_3^2+(2\varpi_3+1)\varpi_1^2\right)\vartheta\Bigg)\ ,$$

which is negative. We find also that

$$\boldsymbol{\xi}^\intercal M\boldsymbol{\eta}=\tau\hat{r}_1\frac{(\delta_0+\vartheta)\mu\vartheta}{2\delta_0^2}\frac{(1-\varpi_1)}{\varpi_3+1}\times\left(\frac{4(1-\varpi_1)(\varpi_3+\varpi_1)\varpi_3}{(2\varpi_3+1)\varpi_1-\varpi_3}\delta_0+\frac{(\varpi_1+2\varpi_1\varpi_3+\varpi_3^2)}{\varpi_3+1}(\delta_0-\vartheta)\right)\ ,$$

which is positive, and so the relevant condition is inequality (18b) and K is positive if and only if

$$\frac{19}{15}\frac{\boldsymbol{\xi}^\intercal M\boldsymbol{\eta}}{k_c^2(1-k_c^2)}<-(\delta_0M_{11}+M_{22})\ .$$

Expressing this inequality only in terms of ϖ_1,ϖ_3 is possible, though simplifying it is arduous and uninformative. However, it is easy to verify that in the case of $\varpi_3=0$ (class **e**) the above inequality holds for all choices of $0<\varpi_1<1$. For class **f** the inequality involves both ω_1 and ω_3 and is represented graphically in the top-right panel of Fig. 2.

3.4. Classes g and h

For classes **g** and **h**, the reaction schemes and stoichiometric conditions to allow Turing instability are

$$\mathbf{g}\begin{cases}2U & \xrightarrow{r_1} n_1''U+m_1V\\ U+V & \xrightarrow{r_2}\emptyset\\ V & \xrightarrow{r_3} n_3U+V\end{cases}$$

subject to: $2(n_1''-2)>m_1>n_1''-2$,

and

$$\mathbf{h}\begin{cases}2U & \xrightarrow{r_1} n_1''U+m_1V\\ U+V & \xrightarrow{r_2}\emptyset\\ V & \xrightarrow{r_3} n_3U+m_3'V\end{cases}$$

subject to: $m_1>n_1''-2\ ,\ n_3>m_3'-1\ ,$
$2(n_1''-2)n_3>m_1n_3+(n_1''-2)(m_3'-1),$

with corresponding mean-field PDE model

$$u_t=D_u\nabla^2u+\hat{r}_3v+\hat{r}_1u^2-r_2uv\ ,$$
$$v_t=D_v\nabla^2v+\hat{r}_3\omega_3v+\hat{r}_1\omega_1u^2-r_2uv\ ,$$

where $\hat{r}_1=(n_1''-2)r_1$, $\hat{r}_3=n_3r_3$, and we define, for these cases,

$$\omega_1:=\frac{m_1}{n_1''-2}\ ,\ \omega_3:=\frac{m_3'-1}{n_3}\ .$$

For the reaction scheme to be Turing-unstable, we must have $0\leqslant\omega_3<1$ and $1<\omega_1<2-\omega_3$. Rescaling $u=u^*+U$, $v=v^*+vV$ about the homogeneous steady state

$$u^*=\frac{\hat{r}_3}{r_2}\frac{\omega_1-\omega_3}{\omega_1-1}\ ,\ v^*=\frac{\hat{r}_1\hat{r}_3}{r_2^2}\frac{(\omega_1-\omega_3)^2}{(\omega_1-1)(1-\omega_3)}\ ,$$

we obtain the nondimensionalised form (19) with

$$\tau=\frac{r_2}{\hat{r}_1\hat{r}_3}\frac{(\omega_1-1)(1-\omega_3)}{(\omega_1-\omega_3)(2-\omega_1-\omega_3)}\ ,$$
$$\nu=\frac{1}{\sqrt{\hat{\rho}}}\sqrt{\frac{\omega_1-\omega_3}{1-\omega_3}\left(2\omega_1-2+\frac{2-\omega_1-\omega_3}{1-\omega_3}\right)},$$
$$\vartheta=\hat{\rho}\frac{\omega_1(1-\omega_3)^2}{(\omega_1-\omega_3)(2-\omega_1-\omega_3)}\ ,$$
$$\mu=\frac{\nu\vartheta}{\omega_1}\ ,$$
$$N=\tau\hat{r}_1\begin{pmatrix}2 & -\hat{\rho}\nu\\ 2\omega_1\nu^{-1} & -\hat{\rho}\end{pmatrix}\ ,\ \hat{\rho}=\frac{r_2}{\hat{r}_1}\ .$$

For these classes

$$M=-\frac{\tau\hat{r}_1}{2\delta_0\vartheta}\begin{pmatrix}4\delta_0\mu\vartheta-\hat{\rho}\omega_1\mu(\delta_0+\vartheta) & -2\hat{\rho}\omega_1\delta_0\mu^2\\ 4\delta_0\vartheta^2-\hat{\rho}\vartheta(\delta_0+\vartheta) & -2\hat{\rho}\delta_0\mu\vartheta\end{pmatrix}\ ,$$

and so

$$\delta_0M_{11}+M_{22}=-\frac{\tau\hat{r}_1\hat{\rho}\mu}{2\vartheta}\times\left(\frac{\omega_1(\omega_1-1)^2(\delta_0+3\vartheta)+3\omega_1(1-\omega_3)^2(\delta_0-\vartheta)}{(\omega_1-\omega_3)(2-\omega_1-\omega_3)}+2(\omega_1-1)\vartheta\right)\ ,$$

which is negative, and

$$\boldsymbol{\xi}^\intercal M\boldsymbol{\eta}=\frac{\tau\hat{r}_1\hat{\rho}}{\vartheta}\frac{\mu(\delta_0+\vartheta)}{2\delta_0}(\omega_1-1)^2\times\left(\frac{\omega_1^2(\delta_0-\vartheta)+2(\omega_1^2-\omega_3^2)\vartheta}{\omega_1(\omega_1-\omega_3)(2-\omega_1-\omega_3)}+\frac{2|\mu|\sqrt{\mu^2-\vartheta}}{\omega_1-1}\right)\ ,$$

which is positive, and so K is positive if and only if inequality (18b) holds:

$$\frac{19}{15}\frac{\boldsymbol{\xi}^\intercal M\boldsymbol{\eta}}{k_c^2(1-k_c^2)}<-(\delta_0M_{11}+M_{22})\ .$$

This inequality does not hold throughout the Turing-unstable region, so K can take either sign. Simplifying the inequality to state it in terms of ω_1 and ω_3 is hypothetically possible, but practically onerous. Even in the simpler case of class **g** for which $\omega_3=0$, there are Turing-unstable reaction schemes for which $K<0$, and the exact condition for class **g** is much simpler to state:

$$K>0\iff\omega_1<\frac{1862-68\sqrt{481}}{225}\approx1.6473\ .$$

This condition for class **g** is illustrated schematically in Fig. 1, and the more complex dependence of sign(K) on ω_1 and ω_3 for class **h** is illustrated in the lower-left plot in Fig. 2.

3.5. Classes i and j

For these two classes, the general reaction schemes and conditions to be Turing-unstable are

$$\mathbf{i}\begin{cases}2U\xrightarrow{r_1}n_1''U+m_1V\\ U+V\xrightarrow{r_2}V\\ V\xrightarrow{r_3}\emptyset\end{cases}\ ,$$

and

$$\mathbf{j}\begin{cases}2U\xrightarrow{r_1}n_1''U+m_1V\\ U+V\xrightarrow{r_2}V\\ V\xrightarrow{r_3}n_3U\end{cases}$$

subject to: $n_1''-2>m_1n_3$,

giving the corresponding mean-field PDE model

$$u_t=D_u\nabla^2u+r_3\varpi_3v+\hat{r}_1\varpi_1u^2-r_2uv\ ,$$
$$v_t=D_v\nabla^2v-r_3v+\hat{r}_1u^2\ ,$$

where we define

$$\varpi_1:=\frac{n_1''-2}{m_1}\ ,\ \varpi_3:=n_3\ .$$

For the reaction scheme to be Turing-unstable we must have $0\leqslant\varpi_3<\varpi_1$. Rescaling $u=u^*+U$, $v=v^*+vV$ about the homogeneous steady state

$$u^*=\frac{r_3}{r_2}(\varpi_1+\varpi_3)\ ,\ v^*=\frac{\hat{r}_1r_3}{r_2^2}(\varpi_1+\varpi_3)^2\ ,$$

we obtain the same nondimensional Eqs. (19) now with

$$\tau=\frac{r_2}{\hat{r}_1r_3}\frac{1}{\varpi_1^2-\varpi_3^2}\ ,$$
$$\nu=\frac{1}{\sqrt{\hat{\rho}}}\sqrt{\frac{2(\varpi_1+\varpi_3)}{\varpi_1}},$$
$$\vartheta=\hat{\rho}\frac{1}{\varpi_1^2-\varpi_3^2}\ ,$$

$$\mu = \nu\varpi_1\vartheta \ ,$$
$$N = \tau\hat{r}_1 \begin{pmatrix} 2\varpi_1 & -\hat{\rho}\nu \\ 2\nu^{-1} & 0 \end{pmatrix} \ , \ \hat{\rho} = \frac{r_2}{\hat{r}_1} \ .$$

In this case we find that

$$M = -\frac{\tau\hat{r}_1}{2\varpi_1\delta_0\vartheta} \begin{pmatrix} 4\varpi_1^2\delta_0\mu\vartheta - \hat{\rho}\mu(\delta_0+\vartheta) & -2\hat{\rho}\delta_0\mu^2 \\ 4\varpi_1^2\delta_0\vartheta^2 & 0 \end{pmatrix}$$

and thus

$$\delta_0 M_{11} + M_{22} = -\frac{\tau\hat{r}_1\mu}{2\varpi_1}\left(2\varpi_1^2\delta_0 + \varpi_3^2(\delta_0+\vartheta) + \varpi_1^2(\delta_0-\vartheta)\right),$$

which is always negative, and

$$\boldsymbol{\xi}^{\mathsf{T}} M\boldsymbol{\eta} = \tau\hat{r}_1 \frac{(\delta_0+\vartheta)\mu\vartheta}{\delta_0} \frac{\sqrt{\varpi_1+\varpi_3}}{\varpi_1-\varpi_3} \times \left(\varpi_1\left(\sqrt{2\varpi_1} - \sqrt{\varpi_1+\varpi_3}\right) + 2\varpi_3\sqrt{\varpi_1+\varpi_3}\right) ,$$

which is positive. Accordingly, K is positive if and only if inequality (18b) holds:

$$\frac{19}{15}\frac{\boldsymbol{\xi}^{\mathsf{T}} M\boldsymbol{\eta}}{k_c^2(1-k_c^2)} < -(\delta_0 M_{11} + M_{22}) \ ,$$

After much algebraic manipulation and simplification, taking into account that $0 \leqslant \varpi_3 < \varpi_1$, this inequality holds if and only if

$$(15\gamma + 38)\sqrt{\gamma} > 53\gamma + 2 \, ,$$

where we introduce $\gamma := (\varpi_1+\varpi_3)/(2\varpi_1)$ for convenience. If we resort to the cubic formula, then this inequality can be further simplified and expressed purely in terms of the ratio ϖ_3/ϖ_1. Within the Turing instability regime it is equivalent to

$$\sqrt{\frac{\varpi_1+\varpi_3}{2\varpi_1}} < \frac{53}{45} + \frac{2\sqrt{1099}}{45}\cos\left(\frac{c_0 - 2\pi}{3}\right) \ , \tag{20}$$

where

$$c_0 := \arccos\left(\frac{19007}{1099\sqrt{1099}}\right),$$

and the right-hand side of inequality (20) evaluates to approximately 0.90973. In particular, for class **i** we have $\varpi_3 = 0$, so the above inequality becomes independent of ϖ_1 and is numerically true; therefore $K > 0$ for all choices of stoichiometry in class **i**. For class **j** the inequality involves both ω_1 and ω_3 and is represented graphically in the lower-centre panel of Fig. 2.

3.6. Class **k**

For the final class of reaction schemes

$$\mathbf{k} \begin{cases} 2U \xrightarrow{r_1} n_1'' U + m_1 V \\ U + V \xrightarrow{r_2} m_2' V \\ V \xrightarrow{r_3} \emptyset \end{cases} ,$$

a Turing instability is feasible, in terms of the existence of open sets of reaction rates and diffusivities, for any choice of stoichiometric product coefficients $n_1'' > 2$, $m_2' > 1$, $m_1 > 0$. The mean-field PDE model is

$$u_t = D_u\nabla^2 u + \hat{r}_1 u^2 - r_2 uv \ ,$$
$$v_t = D_v\nabla^2 v - r_3 v + \hat{r}_1\omega_1 u^2 + r_2\omega_2 uv \ ,$$

where $\hat{r}_1 = r_1(n_1 - 2)$ and

$$\omega_1 := \frac{m_1}{n_1 - 2} \ , \ \omega_2 := m_2' - 1 \ ,$$

satisfying $\omega_1, \omega_2 > 0$. The nonzero homogeneous steady state is

$$u^* = \frac{r_3}{r_2}\frac{1}{\omega_1+\omega_2} \ , \ v^* = \frac{\hat{r}_1 r_3}{r_2^2}\frac{1}{\omega_1+\omega_2} \ ,$$

and the equations are put into the dimensionless form (19) by defining

$$\tau = \frac{r_2}{\hat{r}_1 r_3}(\omega_1+\omega_2) \ ,$$
$$\nu = \frac{1}{\sqrt{\hat{\rho}}}\sqrt{2\omega_1+\omega_2} \ ,$$
$$\vartheta = \hat{\rho}\omega_1 \ ,$$
$$\mu = \hat{\rho}\nu \ ,$$
$$N = \tau\hat{r}_1 \begin{pmatrix} 2 & -\hat{\rho}\nu \\ 2\omega_1\nu^{-1} & \hat{\rho}\omega_2 \end{pmatrix} \ , \ \hat{\rho} = \frac{\hat{r}_2}{\hat{r}_1} \ .$$

Computation yields

$$M = -\frac{\tau\hat{r}_1}{2\delta_0} \begin{pmatrix} 4\delta_0\mu - \mu(\delta_0+\vartheta) & -2\delta_0\mu^2 \\ 4\hat{\rho}\omega_1\delta_0 + \hat{\rho}\omega_2(\delta_0+\vartheta) & 2\hat{\rho}\omega_2\delta_0\mu \end{pmatrix} ,$$

and thus

$$\delta_0 M_{11} + M_{22} = -\frac{\tau\hat{r}_1\mu}{2}\left(2\delta_0 + (\delta_0-\vartheta) + 2\hat{\rho}\omega_2\right) \ ,$$

which is always negative, and

$$\boldsymbol{\xi}^{\mathsf{T}} M\boldsymbol{\eta} = \tau\hat{r}_1\hat{\rho}\frac{(\delta_0+\vartheta)^2\mu}{2\delta_0^2}\sqrt{\frac{\omega_1+\omega_2}{2\omega_1+\omega_2}}\left(\omega_1+\omega_2\right) \ ,$$

which is always positive. By inequality (18b) we have that K is positive if and only if

$$\frac{19}{15} < \frac{3}{2}\sqrt{\frac{2\omega_1+\omega_2}{\omega_1+\omega_2}} + 2 \ ,$$

which is true for all $\omega_1, \omega_2 > 0$, and so K is positive for all reaction schemes in class **k**.

In summary, we have computed the cubic coefficient in the standard weakly nonlinear analysis for each of the 11 classes of minimal reaction schemes for type-I Turing instability. We find that in three classes (**e**, **i**, and **k**) the instability is always supercritical, while in six cases (**a**, **b**, **f**, **g**, **h**, and **j**) there are regions of both supercriticality and subcriticality. As a general rule, the instability is found to be supercritical when $\omega_1 \equiv m_1/(n_1-2)$, i.e. the ratio of the stoichiometric increases in the second and first species due to the reaction $2U \to n_1 U + m_1 V$, is sufficiently small, and subcritical when it is larger. In the remaining two cases (**c** and **d**) there is a degeneracy in the structure of the linear and nonlinear terms caused by the existence of a common factor of u, which means that the sub- or supercriticality of the bifurcation is not determined at this order.

4. Further analysis for classes c and d.

If $\boldsymbol{\xi}^{\mathsf{T}} M\boldsymbol{\eta} = 0$, as we observed in Section 3.2, then the real Ginzburg–Landau amplitude Eq. (16) cannot describe nonzero uniform equilibrium solutions for the amplitude A. In order to capture nonzero steady states, if they exist, we must introduce new scalings in the asymptotic expansion to allow for larger amplitudes. We do this by proposing a new asymptotic expansion for the amplitudes (U, V) while keeping the same scalings as introduced previously for the slow time scale $T = \varepsilon^2 t$ and long length scale $X = \varepsilon x$:

$$\begin{pmatrix} U \\ V \end{pmatrix} = \varepsilon^{\frac{1}{2}}\begin{pmatrix} U_{\frac{1}{2}} \\ V_{\frac{1}{2}} \end{pmatrix} + \varepsilon\begin{pmatrix} U_1 \\ V_1 \end{pmatrix} + \varepsilon^{\frac{3}{2}}\begin{pmatrix} U_{\frac{3}{2}} \\ V_{\frac{3}{2}} \end{pmatrix} + \cdots \ . \tag{21}$$

In this new computation we also impose the additional constraint $\boldsymbol{\xi}^{\mathsf{T}} M\boldsymbol{\eta} = 0$ which is a new condition relating μ and ϑ. We explore the effects of varying μ and ϑ close to this constraint by perturbing them and writing $\mu \mapsto \mu + \varepsilon\mu_1$, $\vartheta \mapsto \vartheta + \varepsilon\vartheta_1$. Substituting this into the governing Eq. (2) we have

$$\varepsilon^{\frac{5}{2}}\partial_T\begin{pmatrix} U_{\frac{1}{2}} \\ V_{\frac{1}{2}} \end{pmatrix} = \mathcal{L}\begin{pmatrix} U \\ V \end{pmatrix} + \varepsilon\begin{pmatrix} 0 & -\mu_1 \\ \mu_1 & -\vartheta_1 \end{pmatrix}\begin{pmatrix} U \\ V \end{pmatrix} + \varepsilon^{\frac{5}{2}}\partial_{XX}\begin{pmatrix} U_{\frac{1}{2}} \\ \delta_0 V_{\frac{1}{2}} \end{pmatrix} + \varepsilon^{\frac{5}{2}}\partial_{xx}\begin{pmatrix} 0 \\ \delta_2 V_{\frac{1}{2}} \end{pmatrix}$$

$$+ 2\varepsilon\partial_{xX}\begin{pmatrix} U \\ \delta_0 V \end{pmatrix} + N\begin{pmatrix} \frac{1}{2}U^2 \\ UV \\ \frac{1}{2}V^2 \end{pmatrix} + \mathcal{O}(\varepsilon^3) \ . \tag{22}$$

Comparing the constraint $\boldsymbol{\xi}^\intercal M\boldsymbol{\eta} = 0$, to Eq. (11), we observe that the two vectors

$$M\boldsymbol{\eta} \quad \text{and} \quad \begin{pmatrix} 1 & 0 \\ 0 & \delta_0 \end{pmatrix}\boldsymbol{\eta}$$

are both orthogonal to $\boldsymbol{\xi}$ and therefore (since these are all non-zero vectors in $\mathbb{R}^2$) they must be scalar multiples of each other. Similarly, the vectors

$$\boldsymbol{\xi}^\intercal M \quad \text{and} \quad \boldsymbol{\xi}^\intercal\begin{pmatrix} 1 & 0 \\ 0 & \delta_0 \end{pmatrix}$$

are also both orthogonal to $\boldsymbol{\eta}$ and so must be multiples of each other. We can therefore write

$$M\boldsymbol{\eta} = \chi_1\begin{pmatrix} 1 & 0 \\ 0 & \delta_0 \end{pmatrix}\boldsymbol{\eta} \ , \ \boldsymbol{\xi}^\intercal M = \chi_2\boldsymbol{\xi}^\intercal\begin{pmatrix} 1 & 0 \\ 0 & \delta_0 \end{pmatrix} \ ,$$

where the scalars χ_1, χ_2 can be computed simply by multiplying these equations by $\boldsymbol{\eta}^\intercal$ and $\boldsymbol{\xi}$, respectively, to obtain

$$\chi_1 = \frac{\boldsymbol{\eta}^\intercal M\boldsymbol{\eta}}{2\delta_0(1-k_c^2)^2} \ , \ \chi_2 = \frac{\boldsymbol{\xi}^\intercal M\boldsymbol{\xi}}{2\delta_0(1-k_c^2)^2} \ . \tag{23}$$

These expressions turn up repeatedly in the asymptotic calculation that follows when we consider terms order by order in solving Eq. (22). Full details of the calculation are presented in Appendix B; in this section we summarise the approach and present the result.

At leading order (which is now $\mathcal{O}(\varepsilon^{1/2})$ with these new scalings) we obtain an eigenvalue equation for the matrix L_1, defined as before, which has the expected solution

$$\begin{pmatrix} U_{\frac{1}{2}} \\ V_{\frac{1}{2}} \end{pmatrix} = (a+\bar{a})\boldsymbol{\eta} \ , \tag{24}$$

where $a(x,X,T) = \exp(ik_c x)A(X,T)$ and, also as before, $A(X,T)$ is an as-yet-undetermined complex-valued amplitude. Proceeding in a similar manner to before, when we arrive at third order (i.e. $\mathcal{O}(\varepsilon^{3/2})$) there is now a new solvability constraint which relates μ_1 and ϑ_1:

$$0 = \boldsymbol{\xi}^\intercal\begin{pmatrix} 0 & -\mu_1 \\ \mu_1 & -\vartheta_1 \end{pmatrix}\boldsymbol{\eta} \iff 2\mu\mu_1 = (1-k_c^2)\vartheta_1 \ ,$$

which enforces the requirement that the change in δ_0 due to the perturbations μ_1, ϑ_1 is only $\mathcal{O}(\varepsilon^2)$, rather than $\mathcal{O}(\varepsilon)$ as might be expected, i.e.

$$\delta_0(\mu+\varepsilon\mu_1, \vartheta+\varepsilon\vartheta_1) = \delta_0(\mu,\vartheta) + \mathcal{O}(\varepsilon^2) \ .$$

An amplitude equation for A is retrieved at fifth order (i.e. $\mathcal{O}(\varepsilon^{5/2})$), where applying the solvability condition yields the cubic-quintic Ginzburg–Landau equation

$$\begin{aligned} A_T = {} & A_{XX} + \delta_2 A - \mu_1(2\chi_2^2 + \chi_1\chi_2 + \chi_1^2)A|A|^2 - \chi_1^2\chi_2(2\chi_2+\chi_1)A|A|^4 \\ & + 2\mu_1 iA_X + \frac{2}{5}\left(2\chi_2^2 + 3\chi_1\chi_2 + 5\chi_1^2\right)iA_X|A|^2 \\ & + \frac{1}{5}\left(-6\chi_2^2 + \chi_1\chi_2 + 5\chi_1^2\right)iA^2\bar{A}_X \ . \end{aligned} \tag{25}$$

At $\mu_1 = 0$, the existence (and stability) of spatially constant solutions depends upon the coefficient of the term $A|A|^4$ which we denote by K_2

$$K_2 := \chi_1^2\chi_2(2\chi_2+\chi_1) \ .$$

If $K_2 > 0$, then stable stripe pattern solutions with $|A| = (\delta_2/K_2)^{1/4}$ bifurcate from the unstable zero amplitude solution for $\delta_2 > 0$, while if $K_2 < 0$ then unstable stripe patterns bifurcate away from the stable zero solution for $\delta_2 < 0$. Away from $\mu_1 = 0$, nonzero stable homogeneous solutions can still exist if

$$\mu_1^2(2\chi_2^2 + \chi_1\chi_2 + \chi_1^2)^2 > 4\delta_2\chi_1^2\chi_2(2\chi_2+\chi_1) \ .$$

In the specific cases of classes **c** and **d**, it is straightforward to compute the numerators of the expressions in (23) directly. We obtain

$$\boldsymbol{\eta}^\intercal M\boldsymbol{\eta} = -\frac{2\tau\hat{r}_1\mu^3}{\delta_0}\left(\delta_0 - \vartheta\right) = 2\boldsymbol{\xi}^\intercal M\boldsymbol{\xi} \ .$$

which implies $\chi_1 = 2\chi_2 \neq 0$. Thus we can further rescale to obtain the amplitude equation

$$A_T = A_{XX} + \delta_2 A - A|A|^4 + \frac{14}{5}iA_X|A|^2 + \frac{4}{5}iA^2\bar{A}_X \ ,$$

which admits stable spatially homogeneous solutions $|A| = \delta_2^{1/4}$ that exist when $\delta_2 > 0$. To summarise, although classes **c** and **d** appear to be degenerate in the sense that the coefficient K in the usual amplitude equation vanishes identically, this more detailed analysis confirms that we should still expect that stable spatially periodic patterns could be generated in these cases.

5. Codimension-two cases in which $K = 0$

As Figs. 1 and 2 clearly illustrate, there are boundary cases in which the cubic coefficient K vanishes at particular values of ω_1 (in classes **a** and **g**), or along specific lines in the (ω_1,ω_3) plane (in classes **b**, **f**, **h** and **j**). At these boundary points and lines, we find that K vanishes because the second factor in Eq. (17) vanishes (and in all cases the first factor $\boldsymbol{\xi}^\intercal M\boldsymbol{\eta}$ remains finite and, in fact, strictly positive). To investigate what happens at these boundaries, we are able to repeat the analysis of the previous subsection in slightly greater generality, using the condition that $K = 0$ but without assuming that $\boldsymbol{\xi}^\intercal M\boldsymbol{\eta}$ vanishes. This results again in amplitude equations of the same form, i.e. the cubic-quintic Ginzburg–Landau equation

$$\begin{aligned} A_T = {} & A_{XX} + \delta_2 A + \mu_1 q_1 A|A|^2 - q_2 A|A|^4 \\ & + 2\mu_1 iA_X + q_3 iA_X|A|^2 + q_4 iA^2\bar{A}_X \ , \end{aligned}$$

where q_1, q_2, q_3 and q_4 are complicated real-valued functions of μ and ϑ. In the special case in which $\boldsymbol{\xi}^\intercal M\boldsymbol{\eta} = 0$ this form reduces to that previously calculated, i.e. Eq. (25). Details of the general calculation are provided in Appendix C. As in the previous case, we focus on determining the sign of q_2 as a function of the stoichiometric effect ratios ω_i for the six relevant classes.

For the four cases that have boundary lines in the (ω_1,ω_3)-plane on which $K = 0$, Fig. 3 plots the sign of q_2 in the (ω_1,ω_3) plane along with dash-dotted lines which correspond directly to the boundaries between the coloured regions in Fig. 2. This allows us to explore the sign of q_2 when $K = 0$, and hence whether we expect the instability to be stabilised at larger amplitudes if K is small and negative, so that the instability is subcritical. The 1-parameter boundary values in classes **a** and **g** may be seen by setting $\omega_3 = 0$ in the corresponding plots for classes **b** and **h** respectively.

We conclude that in cases **a**, **f** and **g**, since $q_2 > 0$ when $K = 0$, that the instability is stabilised by the quintic-order term. Cases **b**, **h** and **j** appear, for very small ω_1, to be even more delicate still.

We remark only that if $q_2 < 0$ along the line on which $K = 0$, then small-amplitude patterned states may well not exist; and if both K and q_2 vanish then a further rescaling may well be required in order to pursue the analysis further; we do not pursue this even more degenerate case here.

6. Numerical simulations

In this section we present numerical simulations in two example cases, in order both to illustrate the calculations presented in previous sections and to validate their predictions. Simulating the example cases for diffusivity ratios δ a little above the Turing instability threshold value, δ_0, confirms that a small-amplitude spatially periodic perturbation to the uniform steady state can settle down to a stripe pattern at later times: see Figs. 4, 6 and 9. In Fig. 4 we use an example from class **a**, corresponding to the PDEs

$$\begin{pmatrix} u_t \\ v_t \end{pmatrix} = \begin{pmatrix} 1 & 0 \\ 0 & \delta \end{pmatrix}\nabla^2\begin{pmatrix} u \\ v \end{pmatrix} + \begin{pmatrix} 1 + 2u^2 - \rho uv \\ 3u^2 - \rho uv \end{pmatrix} \ , \tag{26}$$

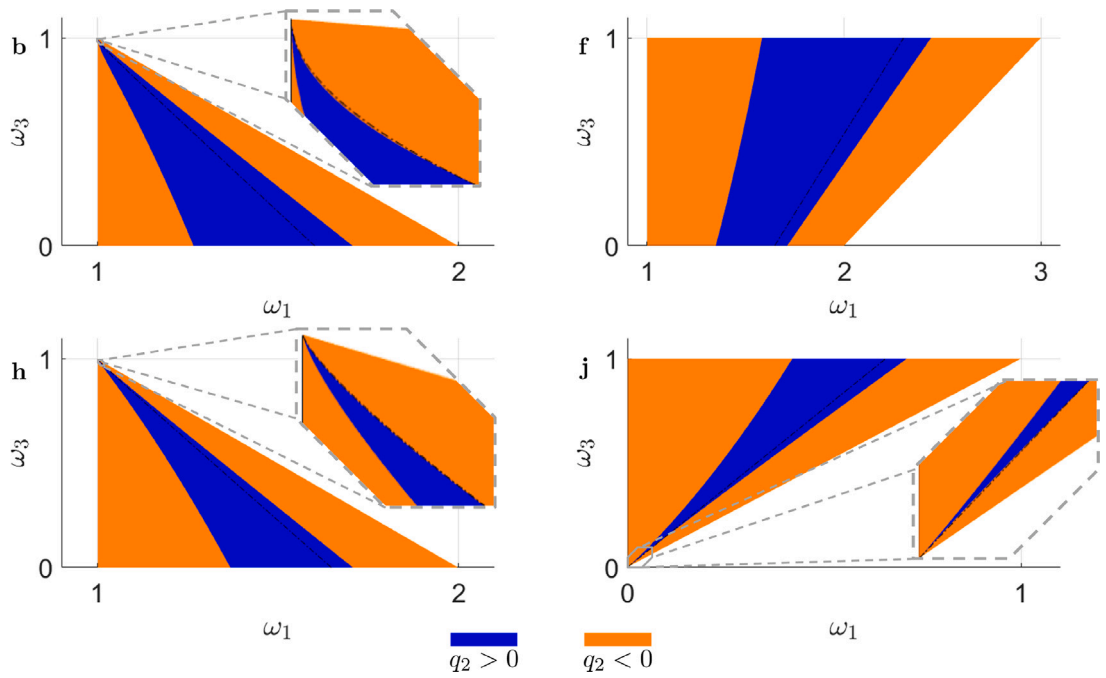

Fig. 3. Sign of q_2 for the four classes of minimal type-I Turing-unstable reaction schemes for which – within the Turing unstable regime – there is a boundary $K = 0$ (dash-dotted line). Enlarged insets of the figures highlight specifically the corners in which the line $K = 0$ crosses into a region where $q_2 < 0$.

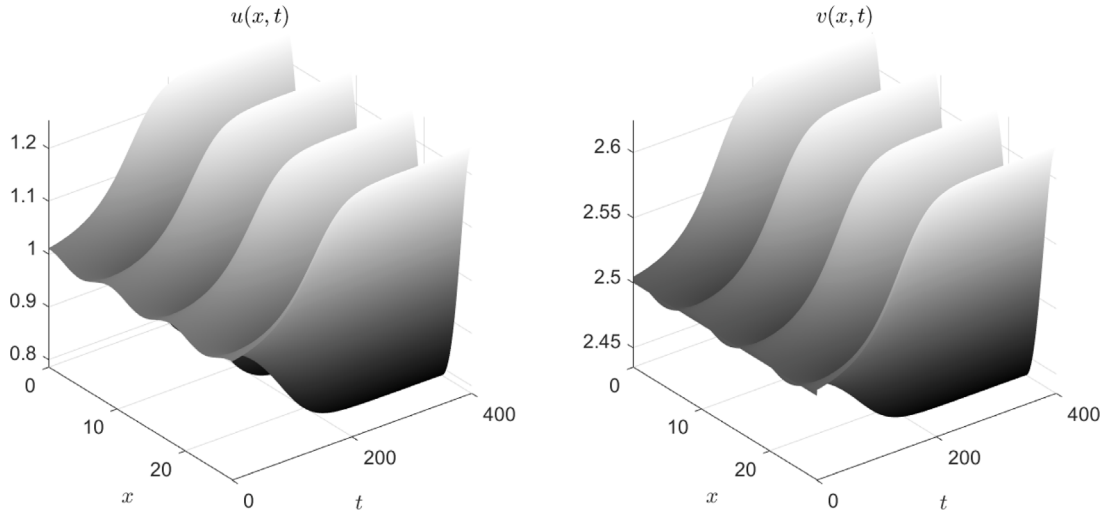

Fig. 4. Numerical simulation of the PDEs (26) corresponding to a reaction scheme from class **a**, in a one-dimensional domain of length $L = 27$ with periodic boundaries, for times $0 \le t \le 400$. We take the initial condition to be the spatially uniform steady state $(u^*, v^*) = (1, 5/2)$ plus a small-amplitude, spatially sinusoidal perturbation to u. The perturbation grows over time in both species (u and v are spatially in phase) before settling to a steady stripe pattern with three peaks – one peak here spans the periodic boundary. Full details of parameter values and initial conditions are given in Appendix D.

where we set $\rho = 6/5$. These support a homogeneous steady state $(u^*, v^*) = (1, 5/2)$ which undergoes a Turing instability when $\delta = \delta_0 \equiv 6(5 + 2\sqrt{6})/5 \approx 11.9$. The Fourier coefficients $\tilde{u}(k,t)$ corresponding to the spatiotemporal profile $u(x,t)$ from Fig. 4 are plotted in Fig. 5. The plot shows that the solution is dominated by the mode that corresponds to the domain being filled by three periods of the periodic pattern. The plot on the right-hand side of Fig. 5 compares the growth rate of this most unstable Fourier mode at early times ($0 \le t \le 120$) to the theoretically-predicted growth rate from the linearised analysis (c.f. Eq. (4)). The agreement is very satisfactory.

Figs. 6 and 7 are generated similarly from numerical simulations of the following PDEs which correspond to an example from class **c**

$$\begin{pmatrix} u_t \\ v_t \end{pmatrix} = \begin{pmatrix} 1 & 0 \\ 0 & \delta \end{pmatrix} \nabla^2 \begin{pmatrix} u \\ v \end{pmatrix} + \begin{pmatrix} u + 2u^2 - \rho uv \\ 3u^2 - \rho uv \end{pmatrix} , \tag{27}$$

where we set $\rho = 11/5$. These PDEs support a homogeneous steady state $(u^*, v^*) = (1, 15/11)$ which undergoes a Turing instability at $\delta = \delta_0 \equiv 11(2 + \sqrt{3})/10 \approx 4.1$. Dispersion relations (4) for both systems, showing the linearised growth rate as a function of perturbation wavenumber are plotted in Fig. 8. It is of interest to note that the PDEs (26) and (27) differ only in one term, yet the first is in class **a** and we find $K > 0$ in this case, while the second is in class **c** for which $K = 0$ always.

For the first system ((26) from class **a**), the weakly nonlinear analysis predicts that steady patterned solutions exist for $\delta > \delta_0$ with a leading order amplitude $|A|$ that scales like $(\delta - \delta_0)^{1/2}$. Specifically, choosing the spatial origin so that the amplitude A is real, from the leading order form of the asymptotic solution we have

$$\begin{pmatrix} U \\ V \end{pmatrix} = 2\varepsilon |A| \cos(k_c x)\boldsymbol{\eta} + \mathcal{O}(\varepsilon^2) ,$$

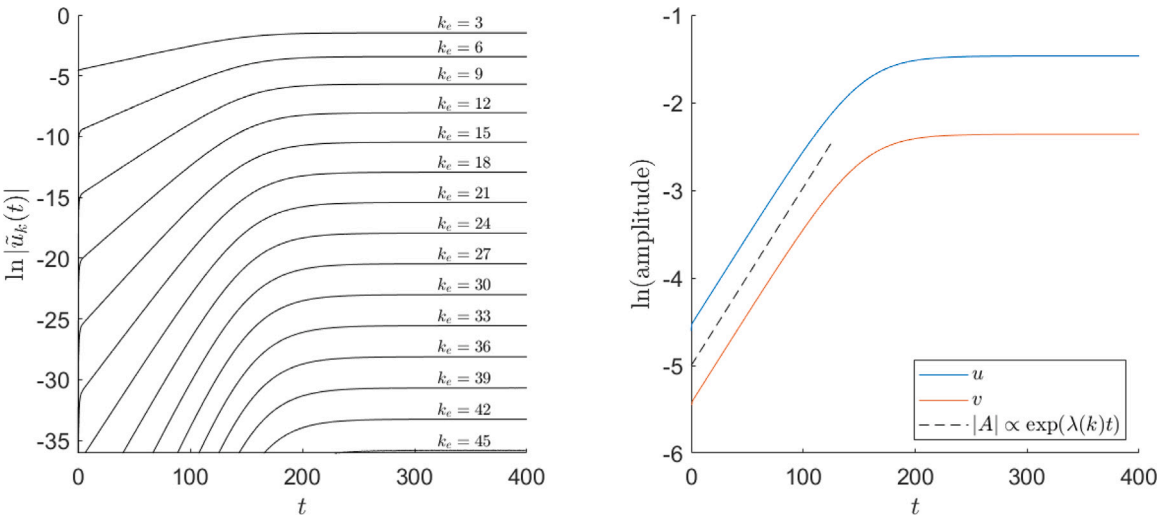

Fig. 5. Fourier mode amplitudes from the simulation shown in Fig. 4. The 'effective wavenumber' k_e gives the number of wavelengths of each perturbation mode contained in the spatial domain. Left: The Fourier amplitudes $\tilde{u}_k(t)$ in the profile $u(x,t)$ plotted on a log scale, the vertical axis is cropped roughly at machine precision: $\exp(-35) \approx 10^{-15}$. Right: The Fourier amplitude of the most unstable wavemode ($k_e = 3$) in both species profiles from the simulation. At early times, the growth of the perturbation matches well the linearised prediction $|A| \propto \exp(\lambda(k_c)t)$.

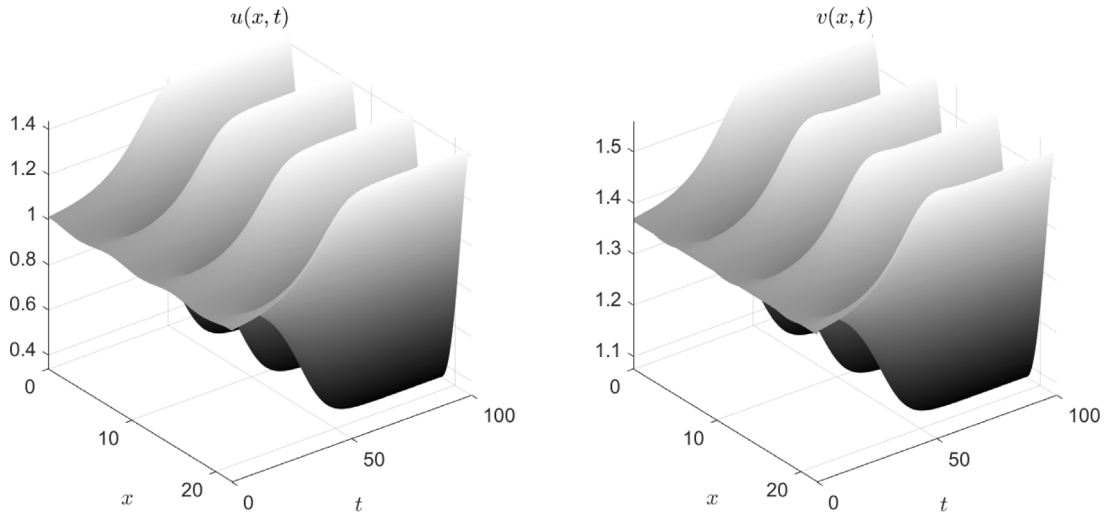

Fig. 6. Numerical simulation of the PDEs (27) corresponding to a reaction scheme from class **c** in a one-dimensional domain of length $L = 22$ with periodic boundaries, for times $0 \leqslant t \leqslant 100$. The uniform steady state $(u^*, v^*) = (1, 15/11)$ is initialised with an added small-amplitude spatially sinusoidal perturbation to u. The perturbation grows over time in both species (spatially in phase) before settling to a steady stripe pattern. Full details of parameter values and initial conditions are given in Appendix D.

where, from Eq. (15) at steady state,

$$\varepsilon|A| = \frac{k_c(1-k_c^2)}{K^{\frac{1}{2}}}(\delta-\delta_0)^{\frac{1}{2}} .$$

Combining these, we have the prediction for the amplitudes $\tilde{U}_{k_c}$, $\tilde{V}_{k_c}$ of the critical wavemode i.e. the coefficients of $\cos(k_c x)$ when U and V are expanded in a Fourier cosine series:

$$\begin{pmatrix}\tilde{U}_{k_c}\\ \tilde{V}_{k_c}\end{pmatrix} = \frac{2k_c(1-k_c^2)}{K^{\frac{1}{2}}}(\delta-\delta_0)^{\frac{1}{2}}\boldsymbol{\eta} + \mathcal{O}(\delta-\delta_0) .$$

For the given stoichiometry ($\omega_1 = 3/2$) and chosen parameter values ($\hat{r}_1 = 2$, $r_2 = \rho = 6/5$, $\hat{r}_3 = 1$), we have $\mu = 3\sqrt{10}/5$, $\vartheta = 6/5$, $k_c = \sqrt{\sqrt{6}-2}$ and

$$N = \begin{pmatrix} 4 & -\frac{3}{5}\sqrt{10} \\ \frac{6}{5}\sqrt{10} & -\frac{6}{5}\end{pmatrix} ,$$

$$M = -\frac{3}{5}\begin{pmatrix} \sqrt{10}+2\sqrt{15} & -6 \\ 6+2\sqrt{6} & -\frac{6}{5}\sqrt{10}\end{pmatrix} ,$$

$$\boldsymbol{\xi}^{\intercal} M \boldsymbol{\eta} = \frac{108}{25}\sqrt{10} .$$

Thus we can evaluate

$$K = \frac{72}{25}(9-2\sqrt{6}) ,$$

yielding the leading order steady state predictions

$$|\tilde{u}_{k_c}| = \left(\frac{5\left(37\sqrt{6}-90\right)}{19}\right)^{\frac{1}{2}}(\delta-\delta_0)^{\frac{1}{2}} , \tag{28a}$$

$$|\tilde{v}_{k_c}| = \frac{5}{6}(3-\sqrt{6})|\tilde{u}_{k_c}| , \tag{28b}$$

where $\tilde{u}_{k_c}$, $\tilde{v}_{k_c}$ are the corresponding Fourier coefficients of the original variables (u, v), and we use moduli such that these predictions still hold under a change of origin.

For the second system ((27) from class **c**), the weakly nonlinear analysis, discussed in Section 4, predicts that $|A|$ instead scales like $(\delta-\delta_0)^{1/4}$ since $K = 0$. Specifically, and again choosing the origin so

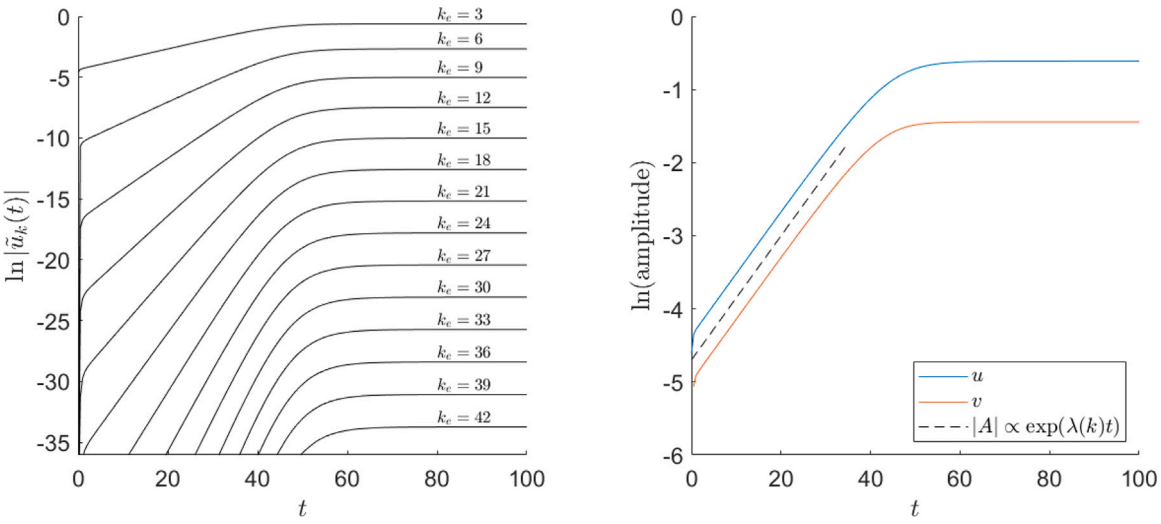

Fig. 7. Fourier mode amplitudes from the simulation shown in Fig. 6. The 'effective wavenumber' k_e gives the number of wavelengths of each perturbation mode contained in the spatial domain. Figure descriptions as in Fig. 5.

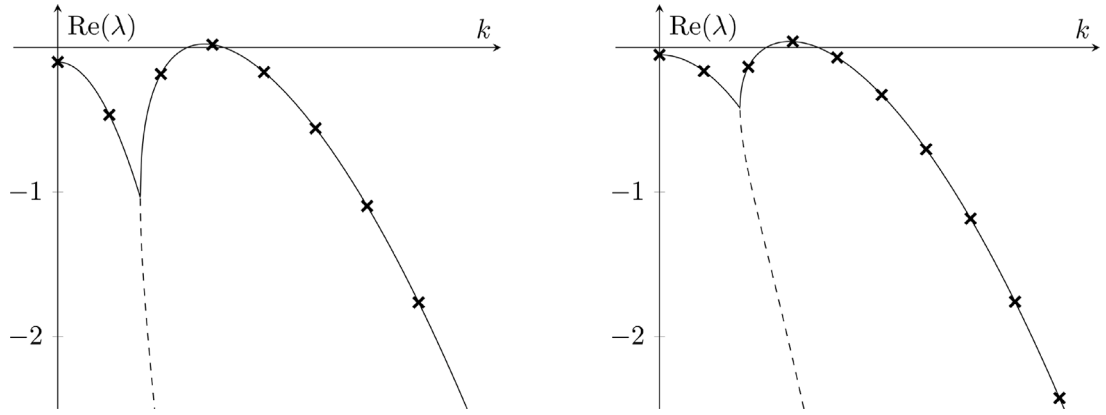

Fig. 8. Dispersion relations displaying the linearised temporal growth rate of a wave perturbation to the homogeneous steady state as a function of the wavenumber – c.f. Eq. (4) – for (left:) the set up used in Fig. 4 and (right:) the set up used in Fig. 6. Crosses mark the growth rates for discrete wavenumbers $k_e = 0, 1, 2, \ldots$ selected by imposing periodic boundary conditions. In each case, only the three-wavelength mode ($k_e = 3$) is linearly unstable. Growth in the other modes, observed in Figs. 5 and 7, is due to nonlinear coupling between modes.

that the amplitude A is real, we have at leading order the solution in the form

$$\begin{pmatrix} U \\ V \end{pmatrix} = 2\varepsilon^{\frac{1}{2}}|A|\cos(k_c x)\boldsymbol{\eta} + \mathcal{O}(\varepsilon) \,,$$

where, from (25), at steady state

$$\varepsilon^{\frac{1}{2}}|A| = \left(\frac{36k_c^6(1-k_c^2)}{25\chi_1^2\chi_2(2\chi_2+\chi_1)\delta_0}\right)^{\frac{1}{4}}(\delta-\delta_0)^{\frac{1}{4}} \,.$$

Combining these, we predict the Fourier amplitudes $(\tilde{U}_{k_c}, \tilde{V}_{k_c})$:

$$\begin{pmatrix} \tilde{U}_{k_c} \\ \tilde{V}_{k_c} \end{pmatrix} = 2\left(\frac{36k_c^6(1-k_c^2)}{25\chi_1^2\chi_2(2\chi_2+\chi_1)\delta_0}\right)^{\frac{1}{4}}(\delta-\delta_0)^{\frac{1}{4}}\boldsymbol{\eta} + \mathcal{O}((\delta-\delta_0)^{\frac{1}{2}}) \,.$$

For the given stoichiometry ($\omega = 3/2$) and chosen parameter values ($\hat{r}_1 = 2$, $r_2 = \rho = 11/5$, $\hat{r}_3 = 1$), we have $\mu = \sqrt{165}/10$, $\vartheta = 11/10$, $k_c = \sqrt{(\sqrt{3}-1)/2}$ and

$$N = \begin{pmatrix} 2 & -\sqrt{165}/10 \\ \sqrt{165}/5 & -11/10 \end{pmatrix} \,,$$

$$\chi_1 = 2\chi_2 = \frac{\sqrt{165}}{10}(1-\sqrt{3}) \,,$$

yielding the leading order steady state predictions

$$|\tilde{u}_{k_c}| = \left(\frac{72(2\sqrt{3}-3)}{55}\right)^{\frac{1}{4}}(\delta-\delta_0)^{\frac{1}{4}} \,, \tag{29a}$$

$$|\tilde{v}_{k_c}| = \frac{5}{11}(3-\sqrt{3})|\tilde{u}_{k_c}| \,, \tag{29b}$$

again expressed in terms of the corresponding Fourier coefficients of the original variables (u, v). Since, in this case, there are no $\exp(\pm ik_c x)$ terms at order $(\delta-\delta_0)^{1/2}$ (i.e. at order ε^2), the error in the predictions given by Eqs. (29) is $\mathcal{O}((\delta-\delta_0)^{3/4})$. Even further, by considering the third order terms in the expansion (21), choosing the origin so that the amplitude A is real and assuming A to be independent of X, we can extract the first correction to these predictions:

$$\begin{pmatrix} \tilde{U}_{k_c} \\ \tilde{V}_{k_c} \end{pmatrix} = 2\varepsilon^{\frac{1}{2}}|A|\left(\boldsymbol{\eta} + \varepsilon\frac{5}{6}\frac{\chi_1^2}{k_c^2}|A|^2(\boldsymbol{\zeta} + c\boldsymbol{\eta})\right) + \mathcal{O}(\varepsilon^{\frac{5}{2}}) \,, \tag{30}$$

where the constant c is not determined by our analysis thus far. If c is chosen correctly, this then allows us to predict how (at steady state) the leading Fourier amplitudes vary with an error of $(\delta-\delta_0)^{5/4}$ – for details see Appendix D. These predictions are validated via a set of numerical simulations to determine the amplitude of the steady-state pattern above the instability threshold, the results of which are plotted in Fig. 9. We observe very strong agreement not just in terms of the

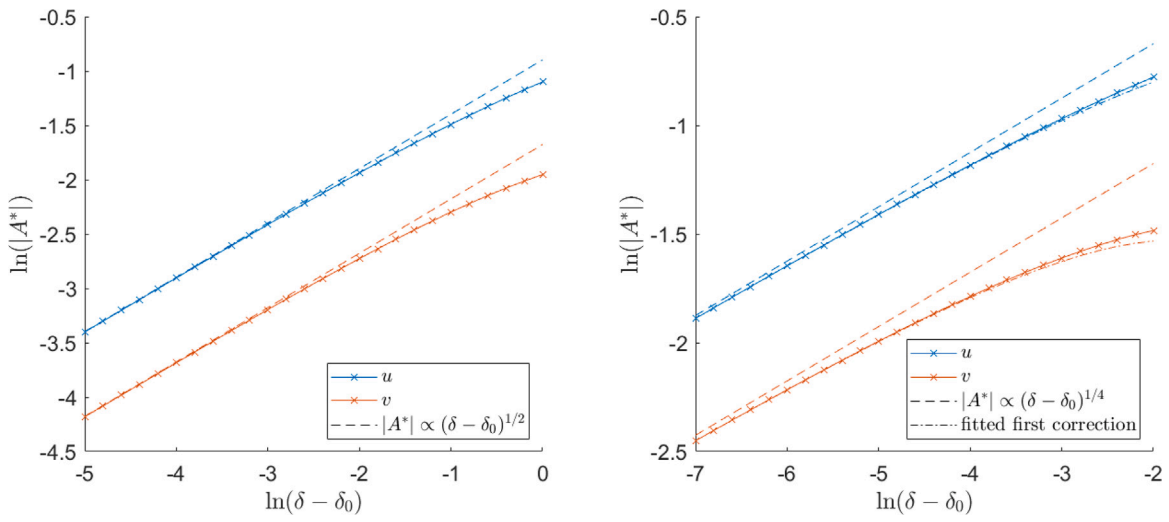

Fig. 9. Steady state amplitude of a planewave perturbation estimated from numerical simulations of an example Turing-unstable reaction scheme from class **a** (left) and from class **c** (right), compared to the predicted leading order steady state amplitudes (dashed lines) $|A|^2 \propto \delta_2$ and $|A|^4 \propto \delta_2$ respectively. Crosses plot the steady state values of the amplitude of the critical Fourier instability mode after the simulation has, up to a tolerance, reached stationarity; i.e. when the difference between two sequential numerical iterates in a chosen vector norm falls below a chosen threshold value. For these simulations we chose the uniform norm $\|\boldsymbol{x}-\boldsymbol{y}\|_\infty = \max_i |x_i - y_i|$ and the threshold value 10^{-8}. Dashed lines show the leading order predictions for the steady state amplitudes as per the weakly nonlinear analysis, c.f. Eqs. (28) and (29); in the right-hand plot the dash-dotted lines show the two-term prediction from Eq. (30) with $c = -2.16$, details of which are provided in Appendix D.

power law scaling of the amplitudes as a function of $\delta - \delta_0$, but also with the exact numerical coefficients predicted by our analysis.

Details of the numerical scheme along with parameter values are provided in Appendix D, but as a brief summary: we simulate the reaction–diffusion PDEs in Fourier space using a Taylor approximation to an exponential time differencing scheme [23,24]. Initial simulations (Figs. 4–7) were performed with a fine spatial mesh and small time step to establish that stable stripe patterns are indeed possible. Sets of simulations over a range of values of δ (Fig. 9) were performed on a coarser spatial mesh with larger time steps and employing a low-pass filter (i.e. aliasing) to ensure numerical stability. Code files are available from the Zenodo digital repository (doi:10.5281/zenodo.14185376) as supplementary material.

7. Conclusions

In this paper we have built directly on our previous work [12] and explored the weakly nonlinear development of the pattern-forming instability that these eleven classes of PDE all, by construction, exhibit.

Curiously, almost every model reaction–diffusion system commonly used in the literature is implicitly much more complicated than the 11 classes explored here which all corrrespond to minimal (i.e. comprising only three individual chemical reactions and two species) schemes, within which each chemical reaction is either zeroth, first or second order.

We have shown here that these reaction–diffusion systems with quadratic reaction dynamics can be sufficient, at least as far as formal weakly nonlinear analysis demonstrates, to exhibit stable Turing patterns. The weakly nonlinear analysis enables us to predict quantitatively the steady state amplitude of patterns, at least sufficiently close to the Turing instability threshold, and we provide, in Fig. 9, verification of this for periodic patterns that have the critical wavenumber k_c. Our analysis also highlights the important role played by the functional form of the reaction terms in prescribing which types of bifurcations can occur as parameter values are varied.

Our main conclusions are as follows. Firstly, that each of the 11 classes of type-I reaction scheme is able to produce small amplitude stable patterns, as long as suitable stoichiometric coefficients are chosen. Of particular interest is that the pattern forming instability is supercritical when the ratio of stoichiometric coefficients $\omega_1 := m_1/(n_1 - 2)$ in the reaction $2U \to n_1 U + m_1 V$ is sufficiently small. Hence a higher level of autocatalytic activity within this reaction, i.e. higher values of n_1, serve to produce more supercritical pattern forming behaviour. We remark that the reaction $2U \to n_1 U + m_1 V$ is common to all 11 classes that we consider here. This commonality was a conclusion from our previous work [12] which derived the 11 minimal classes.

Secondly, we draw attention to the highly degenerate nature of classes **c** and **d**, in which all nonlinear terms contain factors of U. The degenerate nature of the weakly nonlinear analysis in these cases appears not to have been noted before, and appears to be quite subtle, in that it is closely related to the degeneracy in the linear terms which describes the Turing instability, but is algebraically complicated. It may be of interest in future work to see whether similar degeneracies emerge when reaction–diffusion systems with three or more components are considered.

Thirdly, we note that analysis of the boundary cases (within classes **a**, **b**, **f**, **g**, **h**, and **j**) in which the pattern forming instability switches from being supercritical to being subcritical shows that the higher-order terms that appear here have a stabilising effect on the instability, so that even in regions of parameter space where the instability is subcritical (i.e. $K < 0$) we might expect that stable patterns at larger amplitudes exist.

Especially in such cases, the amplitude equations that we derived here have overall a rich bifurcation structure and many more equilibria than just spatially uniform states [25], but a more detailed investigation of these either in the general case of quadratic reaction dynamics or in the specific cases of minimal Turing-unstable reaction schemes is beyond the scope of this paper. In particular we expect that in subcritical cases there are regions of parameter space away from the Turing instability threshold where localised patches of pattern exist and are stable, with bifurcation diagrams containing homoclinic snaking curves.

Another natural direction for future work is the extension of our results in one spatial dimension into a more general analysis of pattern selection in two or more spatial dimensions, for example the relative stability of two-dimensional stripe patterns (corresponding to the one-dimensional patterns studied here) versus spot patterns that arise through the superposition of multiple plane waves.

One important application of these results will be in the study of stochastic reaction–diffusion systems. For an individual-based model of

a scheme of reactions, each of which involves at most two particles, the mean-field approximation to the dynamics yields a PDE system (1). Our work here opens the way for a systematic analysis of so-called 'stochastic Turing patterns' in these systems in comparison to deterministic Turing patterns predictable in the mean field. In particular, the subcritical cases suggest – provided the mean-field predictions hold robustly in the presence of finite-sized effects – the potential for less transient stochastic patterning outside a mean-field Turing-instability range, where fluctuations can repeatedly drive the system between two branches of stable patterns. An exploration of such models and such effects is anticipated as future work.

CRediT authorship contribution statement

F.R. Waters: Writing – review & editing, Writing – original draft, Visualization, Methodology, Investigation, Formal analysis, Conceptualization. **C.A. Yates:** Writing – review & editing, Supervision. **J.H.P. Dawes:** Writing – review & editing, Supervision.

Declaration of competing interest

The authors declare that they have no known competing financial interests or personal relationships that could have appeared to influence the work reported in this paper.

Acknowledgment

F. R. Waters is supported by a scholarship from the EPSRC Centre for Doctoral Training in Statistical Applied Mathematics at Bath (SAMBa), under the project EP/S022945/1.

Appendix A. An alternative expression for K

Here we derive the alternate expression for K given in Eq. (17) at the beginning of Section 3. First, we have that for $p \neq 1$

$$\begin{aligned} L_p^{-1} &= \frac{1}{\det(L_p)} \begin{pmatrix} -p^2\delta_0 k_c^2 - \vartheta & \mu \\ -\mu & -p^2 k_c^2 + 1 \end{pmatrix} \\ &= \frac{1}{(p^2-1)^2\delta_0 k_c^4} \left\{ \frac{1}{1-k_c^2} \begin{pmatrix} -\mu^2 & \mu(1-k_c^2) \\ -\mu(1-k_c^2) & (1-k_c^2)^2 \end{pmatrix} \right. \\ &\quad \left. -(p^2-1)k_c^2 \begin{pmatrix} \delta_0 & 0 \\ 0 & 1 \end{pmatrix} \right\} \\ &= \frac{1}{(p^2-1)^2\delta_0 k_c^4} \left\{ \frac{1}{1-k_c^2} \boldsymbol{\eta}\boldsymbol{\xi}^\intercal - (p^2-1)k_c^2 \begin{pmatrix} \delta_0 & 0 \\ 0 & 1 \end{pmatrix} \right\} , \end{aligned}$$

and so

$$\begin{aligned} L_0^{-1} + \tfrac{1}{2}L_2^{-1} &= \frac{1}{\delta_0 k_c^4} \left\{ \frac{19}{18}\frac{1}{1-k_c^2}\boldsymbol{\eta}\boldsymbol{\xi}^\intercal + \frac{5}{6}k_c^2 \begin{pmatrix} \delta_0 & 0 \\ 0 & 1 \end{pmatrix} \right\} \\ \implies \boldsymbol{\xi}^\intercal M \left(L_0^{-1} + \tfrac{1}{2}L_2^{-1} \right) M\boldsymbol{\eta} &= \frac{1}{\delta_0 k_c^4} \left(\frac{19}{18}\frac{(\boldsymbol{\xi}^\intercal M\boldsymbol{\eta})^2}{1-k_c^2} + \frac{5}{6}k_c^2 \boldsymbol{\xi}^\intercal M \begin{pmatrix} \delta_0 & 0 \\ 0 & 1 \end{pmatrix} M\boldsymbol{\eta} \right) . \end{aligned} \tag{A.1}$$

Now we observe that an arbitrary 2×2 matrix $Z = (Z_{ij})$ can be decomposed as the following sum of four 2×2 matrices:

$$\begin{aligned} Z &= \frac{\delta_0 Z_{11} - Z_{22}}{\delta_0 + \vartheta} \begin{pmatrix} 1 & -\mu \\ \mu & -\vartheta \end{pmatrix} + \frac{\vartheta Z_{11} + Z_{22}}{\delta_0 + \vartheta} \begin{pmatrix} 1 & 0 \\ 0 & \delta_0 \end{pmatrix} \\ &\quad + \begin{pmatrix} 0 & Z_{12} \\ Z_{21} & 0 \end{pmatrix} + \frac{\delta_0 Z_{11} - Z_{22}}{\delta_0 + \vartheta} \begin{pmatrix} 0 & \mu \\ -\mu & 0 \end{pmatrix} , \end{aligned}$$

which yields that

$$\begin{aligned} \boldsymbol{\xi}^\intercal Z\boldsymbol{\eta} &= \boldsymbol{\xi}^\intercal \left\{ \begin{pmatrix} 0 & Z_{12} \\ Z_{21} & 0 \end{pmatrix} + \frac{\delta_0 Z_{11} - Z_{22}}{\delta_0 + \vartheta} \begin{pmatrix} 0 & \mu \\ -\mu & 0 \end{pmatrix} \right\} \boldsymbol{\eta} \\ &= \left\{ \begin{pmatrix} -(1-k_c^2)Z_{21} \\ \mu Z_{12} \end{pmatrix}^\intercal + \frac{\delta_0 Z_{11} - Z_{22}}{\delta_0 + \vartheta} \mu \begin{pmatrix} 1-k_c^2 \\ \mu \end{pmatrix}^\intercal \right\} \begin{pmatrix} -\mu \\ -(1-k_c^2) \end{pmatrix} \\ &= \left\{ \begin{pmatrix} (1-k_c^2)(Z_{12} - Z_{21}) \\ 0 \end{pmatrix}^\intercal + \frac{\delta_0 Z_{11} - Z_{22}}{\delta_0 + \vartheta} \begin{pmatrix} 0 \\ 2\mu^2 \end{pmatrix}^\intercal \right\} \begin{pmatrix} -\mu \\ -(1-k_c^2) \end{pmatrix} \\ &= (1-k_c^2) \begin{pmatrix} Z_{12} - Z_{21} \\ \delta_0 Z_{11} - Z_{22} \end{pmatrix}^\intercal \boldsymbol{\eta} . \end{aligned}$$

By directly multiplying the matrices we also observe that

$$M \begin{pmatrix} \delta_0 & 0 \\ 0 & 1 \end{pmatrix} M = \begin{pmatrix} \delta_0 M_{11}^2 + M_{12}M_{21} & (\delta_0 M_{11} + M_{22})M_{12} \\ (\delta_0 M_{11} + M_{22})M_{21} & \delta_0 M_{12}M_{21} + M_{22}^2 \end{pmatrix} ,$$

and so, combining these results we then have that

$$\begin{aligned} \boldsymbol{\xi}^\intercal M \begin{pmatrix} \delta_0 & 0 \\ 0 & 1 \end{pmatrix} M\boldsymbol{\eta} &= (1-k_c^2) \begin{pmatrix} (\delta_0 M_{11} + M_{22})(M_{12} - M_{21}) \\ \delta_0^2 M_{11}^2 - M_{22}^2 \end{pmatrix}^\intercal \boldsymbol{\eta} \\ &= (1-k_c^2)(\delta_0 M_{11} + M_{22}) \begin{pmatrix} M_{12} - M_{21} \\ \delta_0 M_{11} - M_{22} \end{pmatrix}^\intercal \boldsymbol{\eta} \\ &= (\delta_0 M_{11} + M_{22}) \boldsymbol{\xi}^\intercal M\boldsymbol{\eta} . \end{aligned}$$

Using this result for the last term on the right-hand side of (A.1) then yields

$$\begin{aligned} K &= -\boldsymbol{\xi}^\intercal M \left(L_0^{-1} + \tfrac{1}{2}L_2^{-1} \right) M\boldsymbol{\eta} \\ &= -\frac{1}{\delta_0 k_c^4} \left(\frac{19}{18}\frac{(\boldsymbol{\xi}^\intercal M\boldsymbol{\eta})^2}{1-k_c^2} + \frac{5}{6}k_c^2(\delta_0 M_{11} + M_{22})\boldsymbol{\xi}^\intercal M\boldsymbol{\eta} \right) \\ &= -\frac{5}{6}\frac{\boldsymbol{\xi}^\intercal M\boldsymbol{\eta}}{\delta_0 k_c^2} \left(\frac{19}{15}\frac{\boldsymbol{\xi}^\intercal M\boldsymbol{\eta}}{k_c^2(1-k_c^2)} + \delta_0 M_{11} + M_{22} \right) , \end{aligned}$$

which is the expression for K stated at the start of Section 3.

Appendix B. Derivation of the quintic Ginzburg–Landau equation in the special case in which $\boldsymbol{\xi}^\intercal M\boldsymbol{\eta}$ vanishes

With the asymptotic scalings introduced at the start of Section 4, including the perturbations to μ and ϑ given by $\mu \mapsto \mu + \varepsilon\mu_1$ and $\vartheta \mapsto \vartheta + \varepsilon\vartheta_1$, the scaled reaction–diffusion equations become

$$\begin{aligned} \varepsilon^{\frac{5}{2}}\partial_T \begin{pmatrix} U_{\frac{1}{2}} \\ V_{\frac{1}{2}} \end{pmatrix} &= \mathcal{L} \begin{pmatrix} U \\ V \end{pmatrix} + \varepsilon \begin{pmatrix} 0 & -\mu_1 \\ \mu_1 & -\vartheta_1 \end{pmatrix} \begin{pmatrix} U \\ V \end{pmatrix} + (2\varepsilon\partial_{xX} + \varepsilon^2\partial_{XX}) \begin{pmatrix} U \\ \delta_0 V \end{pmatrix} \\ &\quad + \varepsilon^{\frac{5}{2}}\partial_{xx} \begin{pmatrix} 0 \\ \delta_2 V_{\frac{1}{2}} \end{pmatrix} + N \begin{pmatrix} \frac{1}{2}U^2 \\ UV \\ \frac{1}{2}V^2 \end{pmatrix} + \mathcal{O}(\varepsilon^3) , \end{aligned}$$

which when separated by powers of ε yield the following at successive orders

$$\begin{aligned} \mathcal{O}(\varepsilon) :\ \mathbf{0} &= \mathcal{L} \begin{pmatrix} U_1 \\ V_1 \end{pmatrix} + N \begin{pmatrix} \frac{1}{2}U_{\frac{1}{2}}^2 \\ U_{\frac{1}{2}}V_{\frac{1}{2}} \\ \frac{1}{2}V_{\frac{1}{2}}^2 \end{pmatrix} , \\ \mathcal{O}(\varepsilon^{\frac{3}{2}}) :\ \mathbf{0} &= \mathcal{L} \begin{pmatrix} U_{\frac{3}{2}} \\ V_{\frac{3}{2}} \end{pmatrix} + \begin{pmatrix} 0 & -\mu_1 \\ \mu_1 & -\vartheta_1 \end{pmatrix} \begin{pmatrix} U_{\frac{1}{2}} \\ V_{\frac{1}{2}} \end{pmatrix} \\ &\quad + 2\partial_{xX} \begin{pmatrix} U_{\frac{1}{2}} \\ \delta_0 V_{\frac{1}{2}} \end{pmatrix} + N \begin{pmatrix} U_{\frac{1}{2}}U_1 \\ U_{\frac{1}{2}}V_1 + U_1 V_{\frac{1}{2}} \\ V_{\frac{1}{2}}V_1 \end{pmatrix} , \\ \mathcal{O}(\varepsilon^2) :\ \mathbf{0} &= \mathcal{L} \begin{pmatrix} U_2 \\ V_2 \end{pmatrix} + \begin{pmatrix} 0 & -\mu_1 \\ \mu_1 & -\vartheta_1 \end{pmatrix} \begin{pmatrix} U_1 \\ V_1 \end{pmatrix} \\ &\quad + 2\partial_{xX} \begin{pmatrix} U_1 \\ \delta_0 V_1 \end{pmatrix} + N \begin{pmatrix} U_{\frac{1}{2}}U_{\frac{3}{2}} \\ U_{\frac{1}{2}}V_{\frac{3}{2}} + U_{\frac{3}{2}}V_{\frac{1}{2}} \\ V_{\frac{1}{2}}V_{\frac{3}{2}} \end{pmatrix} + N \begin{pmatrix} \frac{1}{2}U_1^2 \\ U_1 V_1 \\ \frac{1}{2}V_1^2 \end{pmatrix} , \end{aligned}$$

with an amplitude equation to be found at fifth order from the solvability condition. Given the leading order solution (24), we have

$$\mathcal{L} \begin{pmatrix} U_1 \\ V_1 \end{pmatrix} = -\frac{1}{2}(a + \bar{a})^2 M\boldsymbol{\eta}$$

$$\implies \begin{pmatrix} U_1 \\ V_1 \end{pmatrix} = -\left(|a|^2 L_0^{-1} + \frac{1}{2}(a^2+\bar{a}^2) L_2^{-1} \right) M\boldsymbol{\eta} \,,$$

and so

$$\mathcal{L}\begin{pmatrix} U_{\frac{3}{2}} \\ V_{\frac{3}{2}} \end{pmatrix} = -(a+\bar{a}) \begin{pmatrix} 0 & -\mu_1 \\ \mu_1 & -\vartheta_1 \end{pmatrix} \boldsymbol{\eta} - 2ik_c(a_X - \bar{a}_X) \begin{pmatrix} 1 & 0 \\ 0 & \delta_0 \end{pmatrix} \boldsymbol{\eta} + (a+\bar{a})|a|^2 M \left(L_0^{-1} + \tfrac{1}{2} L_2^{-1} \right) M\boldsymbol{\eta} + \frac{1}{2}(a^3+\bar{a}^3) M L_2^{-1} M\boldsymbol{\eta} \,.$$

Imposing the usual solvability condition at order $\varepsilon^{3/2}$ results in a new constraint:

$$0 = \boldsymbol{\xi}^{\intercal} \begin{pmatrix} 0 & -\mu_1 \\ \mu_1 & -\vartheta_1 \end{pmatrix} \boldsymbol{\eta} \quad \text{i.e.} \quad 2\mu\mu_1 = (1-k_c^2)\vartheta_1 \,, \tag{B.1}$$

which corresponds to the constraint that $\delta_0(\mu+\varepsilon\mu_1, \vartheta+\varepsilon\vartheta_1) = \delta_0(\mu,\vartheta) + \mathcal{O}(\varepsilon^2)$, i.e. even though we are perturbing μ and ϑ by an $\mathcal{O}(\varepsilon)$ amount, we do this in such a way that δ is only $\mathcal{O}(\varepsilon^2)$ away from criticality. We shall assume that μ_1, and ϑ_1 are chosen such that (B.1) holds, and note that this constraint also implies that

$$\begin{pmatrix} 0 & -\mu_1 \\ \mu_1 & -\vartheta_1 \end{pmatrix} \boldsymbol{\eta} = \frac{-(1-k_c^2)\mu_1}{\mu} \begin{pmatrix} 1 & 0 \\ 0 & \delta_0 \end{pmatrix} \boldsymbol{\eta}$$

$$\text{and} \quad \boldsymbol{\xi}^{\intercal} \begin{pmatrix} 0 & -\mu_1 \\ \mu_1 & -\vartheta_1 \end{pmatrix} = \frac{-(1-k_c^2)\mu_1}{\mu} \boldsymbol{\xi}^{\intercal} \begin{pmatrix} 1 & 0 \\ 0 & \delta_0 \end{pmatrix} \,, \tag{B.2}$$

and thus the second order solution is in fact

$$\begin{pmatrix} U_1 \\ V_1 \end{pmatrix} = -\frac{\chi_1}{k_c^2} \left(|a|^2 - \frac{1}{6}(a^2+\bar{a}^2) \right) \boldsymbol{\eta} \,,$$

where χ_1 is as defined in Eq. (23) in Section 4. Substituting this into the expansion at $\mathcal{O}(\varepsilon^{3/2})$ and solving, we find that

$$\begin{pmatrix} U_{\frac{3}{2}} \\ V_{\frac{3}{2}} \end{pmatrix} = (b+\bar{b})\boldsymbol{\zeta} + \frac{1}{48}\frac{\chi_1^2}{k_c^4}(a^3+\bar{a}^3)\boldsymbol{\eta} \,,$$

where

$$b = \frac{(1-k_c^2)\mu_1}{\mu} a - 2ik_c a_X + \frac{5}{6}\frac{\chi_1^2}{k_c^2} a|a|^2 \,.$$

We recall that every factor of $a(X,T)$ is implicitly multiplied by the short-lengthscale term $e^{ik_c x}$ which is omitted for clarity. The fourth order terms give

$$\mathcal{L}\begin{pmatrix} U_2 \\ V_2 \end{pmatrix} = -\begin{pmatrix} 0 & -\mu_1 \\ \mu_1 & -\vartheta_1 \end{pmatrix} \begin{pmatrix} U_1 \\ V_1 \end{pmatrix} - 2\partial_{xX} \begin{pmatrix} U_1 \\ \delta_0 V_1 \end{pmatrix} - N \begin{pmatrix} U_{\frac{1}{2}} U_{\frac{3}{2}} \\ U_{\frac{1}{2}} V_{\frac{3}{2}} + U_{\frac{3}{2}} V_{\frac{1}{2}} \\ V_{\frac{1}{2}} V_{\frac{3}{2}} \end{pmatrix} - N \begin{pmatrix} \frac{1}{2}U_1^2 \\ U_1 V_1 \\ \frac{1}{2}V_1^2 \end{pmatrix} \,, \tag{B.3}$$

but we can avoid solving this in full by looking ahead to the fifth order terms:

$$\partial_T \begin{pmatrix} U_{\frac{1}{2}} \\ V_{\frac{1}{2}} \end{pmatrix} = \mathcal{L}\begin{pmatrix} U_{\frac{5}{2}} \\ V_{\frac{5}{2}} \end{pmatrix} + \begin{pmatrix} 0 & -\mu_1 \\ \mu_1 & -\vartheta_1 \end{pmatrix} \begin{pmatrix} U_{\frac{3}{2}} \\ V_{\frac{3}{2}} \end{pmatrix} + 2\partial_{xX} \begin{pmatrix} U_{\frac{3}{2}} \\ \delta_0 V_{\frac{3}{2}} \end{pmatrix} + \partial_{XX} \begin{pmatrix} U_{\frac{1}{2}} \\ \delta_0 V_{\frac{1}{2}} \end{pmatrix} + \partial_{xx} \begin{pmatrix} 0 \\ \delta_2 V_{\frac{1}{2}} \end{pmatrix} + (a+\bar{a}) M \begin{pmatrix} U_2 \\ V_2 \end{pmatrix} + N \begin{pmatrix} U_1 U_{\frac{3}{2}} \\ U_1 V_{\frac{3}{2}} + U_{\frac{3}{2}} V_1 \\ V_1 V_{\frac{3}{2}} \end{pmatrix} \,.$$

We see that, when we impose the solvability condition, the fourth order solution (U_2, V_2) will feature only through the inner product $\boldsymbol{\xi}^{\intercal} M (U_2, V_2)^{\intercal}$, and so any terms in $(U_2, V_2)^{\intercal}$ that are parallel to $\boldsymbol{\eta}$ do not contribute to the solvability condition. In fact, most of the terms on the right-hand side of Eq. (B.3) are parallel to $M\boldsymbol{\eta}$, yielding terms parallel to $\boldsymbol{\eta}$ when the linear operator is inverted. The solution at fourth order is then found to yield

$$\boldsymbol{\xi}^{\intercal} M \begin{pmatrix} U_2 \\ V_2 \end{pmatrix} = -(a\bar{b}+\bar{a}b)\boldsymbol{\xi}^{\intercal} M L_0^{-1} M\boldsymbol{\zeta} - (ab+\bar{a}\bar{b})\boldsymbol{\xi}^{\intercal} M L_2^{-1} M\boldsymbol{\zeta} = \frac{\chi_2^2}{k_c^2}\delta_0(1-k_c^2)(a\bar{b}+\bar{a}b) - \frac{\chi_2^2}{3k_c^2}\delta_0(1-k_c^2)(ab+\bar{a}\bar{b}) \,.$$

Substituting all lower orders into the fifth order equation, after some simplification, the solvability condition at fifth order is

$$\begin{aligned} \frac{\delta_0 - 1}{k_c^2} A_T = {} & \frac{4\delta_0}{1-k_c^2} A_{XX} + \left(\delta_2 - \frac{\mu_1^2}{k_c^2(1-k_c^2)} \right) A \\ & - \frac{5\mu_1\delta_0}{6\mu k_c^4} \left(2\chi_2^2 + \chi_1\chi_2 + \chi_1^2 \right) A|A|^2 \\ & - \frac{25\chi_1^2\chi_2\delta_0}{36k_c^6(1-k_c^2)} \left(2\chi_2 + \chi_1 \right) A|A|^4 + 4\frac{\mu_1\delta_0}{\mu k_c} iA_X \\ & + \frac{2\delta_0}{3k_c^3(1-k_c^2)} \left(2\chi_2^2 + 3\chi_1\chi_2 + 5\chi_1^2 \right) iA_X|A|^2 \\ & + \frac{\delta_0}{3k_c^3(1-k_c^2)} \left(-6\chi_2^2 + \chi_1\chi_2 + 5\chi_1^2 \right) iA^2\bar{A}_X \,. \end{aligned}$$

This can be presented more conveniently by introducing the scaled variables

$$X = \left(\frac{4\delta_0}{1-k_c^2} \right)^{\frac{1}{2}} \hat{X} \,, \quad T = \frac{\delta_0 - 1}{k_c^2} \hat{T} \,, \quad A = \left(\frac{25\delta_0}{36k_c^6(1-k_c^2)} \right)^{-\frac{1}{4}} \hat{A} \,,$$

and using new bifurcation parameters

$$\hat{\mu}_1 := \frac{\sqrt{\delta_0(1-k_c^2)}}{\mu k_c} \mu_1 \,, \quad \hat{\delta}_2 := \delta_2 - \frac{\mu_1^2}{k_c^2(1-k_c^2)} \,.$$

Neglecting $\hat{}$s we get

$$\begin{aligned} A_T = {} & A_{XX} + \delta_2 A - \mu_1 \left(2\chi_2^2 + \chi_1\chi_2 + \chi_1^2 \right) A|A|^2 - \chi_1^2\chi_2 \left(2\chi_2 + \chi_1 \right) A|A|^4 \\ & + 2\mu_1 iA_X + \frac{2}{5} \left(2\chi_2^2 + 3\chi_1\chi_2 + 5\chi_1^2 \right) iA_X|A|^2 \\ & + \frac{1}{5} \left(-6\chi_2^2 + \chi_1\chi_2 + 5\chi_1^2 \right) iA^2\bar{A}_X \,, \end{aligned}$$

which is the quintic Ginzburg–Landau Eq. (25) given at the end of Section 4.

Appendix C. Derivation of the quintic Ginzburg–Landau equation in the general case in which $K = 0$

In general $K = 0$ if and only if $\boldsymbol{\xi}^{\intercal} M (L_0^{-1} + \frac{1}{2} L_2^{-1}) M\boldsymbol{\eta} = 0$. If this holds, then by comparing to Eq. (11), we can write

$$M(L_0^{-1} + \tfrac{1}{2}L_2^{-1}) M\boldsymbol{\eta} = \psi_1 \begin{pmatrix} 1 & 0 \\ 0 & \delta_0 \end{pmatrix} \boldsymbol{\eta}$$

$$\text{and} \quad \boldsymbol{\xi}^{\intercal} M(L_0^{-1} + \tfrac{1}{2}L_2^{-1}) M = \psi_2 \boldsymbol{\xi}^{\intercal} \begin{pmatrix} 1 & 0 \\ 0 & \delta_0 \end{pmatrix} \,,$$

where

$$\psi_1 = \frac{\boldsymbol{\eta}^{\intercal} M(L_0^{-1} + \frac{1}{2}L_2^{-1}) M\boldsymbol{\eta}}{\boldsymbol{\eta}^{\intercal} \begin{pmatrix} 1 & 0 \\ 0 & \delta_0 \end{pmatrix} \boldsymbol{\eta}} \quad \text{and} \quad \psi_2 = \frac{\boldsymbol{\xi}^{\intercal} M(L_0^{-1} + \frac{1}{2}L_2^{-1}) M\boldsymbol{\xi}}{\boldsymbol{\xi}^{\intercal} \begin{pmatrix} 1 & 0 \\ 0 & \delta_0 \end{pmatrix} \boldsymbol{\xi}} \,.$$

Equipped with these, but burdened with a more general form for the second and third order solutions, we can proceed similarly to before, picking back up the analysis from Appendix B up to Eq. (B.2). Now

$$\begin{pmatrix} U_1 \\ V_1 \end{pmatrix} = -|a|^2 L_0^{-1} M\boldsymbol{\eta} - \frac{1}{2}(a^2+\bar{a}^2) L_2^{-1} M\boldsymbol{\eta} \,,$$

and

$$\begin{pmatrix} U_{\frac{3}{2}} \\ V_{\frac{3}{2}} \end{pmatrix} = (b+\bar{b})\boldsymbol{\zeta} + \frac{1}{2}(a^3+\bar{a}^3) L_3^{-1} M L_2^{-1} M\boldsymbol{\eta} \,,$$

where

$$b = a\frac{(1-k_c^2)\mu_1}{\mu} - 2ik_c a_X + \psi_1 a|a|^2 \,.$$

Then solving the fourth order equation explicitly gives

$$\begin{aligned}\begin{pmatrix}U_2\\V_2\end{pmatrix} &= |a|^2 L_0^{-1}\begin{pmatrix}0 & -\mu_1\\ \mu_1 & -\vartheta_1\end{pmatrix} L_0^{-1} M\boldsymbol{\eta} - (a\bar{b}+\bar{a}b) L_0^{-1} M\boldsymbol{\zeta} - |a|^4 \boldsymbol{y}^{(0)}\\ &\quad + \frac{1}{2}(a^2+\bar{a}^2) L_2^{-1}\begin{pmatrix}0 & -\mu_1\\ \mu_1 & -\vartheta_1\end{pmatrix} L_2^{-1} M\boldsymbol{\eta}\\ &\quad + 4ik_c(aa_X - \bar{a}\bar{a}_X) L_2^{-1}\begin{pmatrix}1 & 0\\ 0 & \delta_0\end{pmatrix} L_2^{-1} M\boldsymbol{\eta}\\ &\quad - (ab+\bar{a}\bar{b}) L_2^{-1} M\boldsymbol{\zeta} - (a^2+\bar{a}^2)|a|^2 \boldsymbol{y}^{(2)} - (a^4+\bar{a}^4)\boldsymbol{y}^{(4)}\,,\end{aligned}$$

where

$$\begin{aligned}\boldsymbol{y}^{(0)} &= \frac{1}{2} L_0^{-1} N\begin{pmatrix}(L_0^{-1}M\boldsymbol{\eta})_1 & 0\\ (L_0^{-1}M\boldsymbol{\eta})_2 & (L_0^{-1}M\boldsymbol{\eta})_1\\ 0 & (L_0^{-1}M\boldsymbol{\eta})_2\end{pmatrix} L_0^{-1} M\boldsymbol{\eta}\\ &\quad + \frac{1}{4} L_0^{-1} N\begin{pmatrix}(L_2^{-1}M\boldsymbol{\eta})_1 & 0\\ (L_2^{-1}M\boldsymbol{\eta})_2 & (L_2^{-1}M\boldsymbol{\eta})_1\\ 0 & (L_2^{-1}M\boldsymbol{\eta})_2\end{pmatrix} L_2^{-1} M\boldsymbol{\eta},\\ \boldsymbol{y}^{(2)} &= \frac{1}{2} L_2^{-1} M L_3^{-1} M L_2^{-1} M\boldsymbol{\eta} + \frac{1}{2} L_2^{-1} N\begin{pmatrix}(L_0^{-1}M\boldsymbol{\eta})_1 & 0\\ (L_0^{-1}M\boldsymbol{\eta})_2 & (L_0^{-1}M\boldsymbol{\eta})_1\\ 0 & (L_0^{-1}M\boldsymbol{\eta})_2\end{pmatrix} L_2^{-1} M\boldsymbol{\eta},\\ \boldsymbol{y}^{(4)} &= \frac{1}{2} L_4^{-1} M L_3^{-1} M L_2^{-1} M\boldsymbol{\eta} + \frac{1}{8} L_4^{-1} N\begin{pmatrix}(L_2^{-1}M\boldsymbol{\eta})_1 & 0\\ (L_2^{-1}M\boldsymbol{\eta})_2 & (L_2^{-1}M\boldsymbol{\eta})_1\\ 0 & (L_2^{-1}M\boldsymbol{\eta})_2\end{pmatrix} L_2^{-1} M\boldsymbol{\eta}.\end{aligned}$$

Finally, the solvability condition at fifth order is

$$\begin{aligned}\boldsymbol{\xi}^{\intercal}\boldsymbol{\eta}(a_T+\bar{a}_T) &= \boldsymbol{\xi}^{\intercal}\begin{pmatrix}0 & -\mu_1\\ \mu_1 & -\vartheta_1\end{pmatrix}\boldsymbol{\zeta}(b+\bar{b})\\ &\quad + 2ik_c\boldsymbol{\xi}^{\intercal}\begin{pmatrix}1 & 0\\ 0 & \delta_0\end{pmatrix}\boldsymbol{\zeta}(b_X-\bar{b}_X) - \delta_2 k_c^2(1-k_c^2)^2(a+\bar{a})\\ &\quad + P_1(a+\bar{a})|a|^2 + P_2(b+\bar{b})|a|^2 + P_3(a^2\bar{b}+\bar{a}^2 b)\\ &\quad + P_4(a+\bar{a})|a|^4 + ik_c P_5(a_X-\bar{a}_X)|a|^2\,,\end{aligned} \tag{C.1}$$

where

$$\begin{aligned}P_1 &= \boldsymbol{\xi}^{\intercal} M L_0^{-1}\begin{pmatrix}0 & -\mu_1\\ \mu_1 & -\vartheta_1\end{pmatrix} L_0^{-1} M\boldsymbol{\eta} + \frac{1}{2}\boldsymbol{\xi}^{\intercal} M L_2^{-1}\begin{pmatrix}0 & -\mu_1\\ \mu_1 & -\vartheta_1\end{pmatrix} L_2^{-1} M\boldsymbol{\eta}\,,\\ P_2 &= -\boldsymbol{\xi}^{\intercal} M L_0^{-1} M\boldsymbol{\zeta} - \boldsymbol{\xi}^{\intercal} M L_2^{-1} M\boldsymbol{\zeta} - \boldsymbol{\xi}^{\intercal} N\begin{pmatrix}(L_0^{-1}M\boldsymbol{\eta})_1 & 0\\ (L_0^{-1}M\boldsymbol{\eta})_2 & (L_0^{-1}M\boldsymbol{\eta})_1\\ 0 & (L_0^{-1}M\boldsymbol{\eta})_2\end{pmatrix}\boldsymbol{\zeta}\,,\\ P_3 &= -\boldsymbol{\xi}^{\intercal} M L_0^{-1} M\boldsymbol{\zeta} - \frac{1}{2}\boldsymbol{\xi}^{\intercal} N\begin{pmatrix}(L_2^{-1}M\boldsymbol{\eta})_1 & 0\\ (L_2^{-1}M\boldsymbol{\eta})_2 & (L_2^{-1}M\boldsymbol{\eta})_1\\ 0 & (L_2^{-1}M\boldsymbol{\eta})_2\end{pmatrix}\boldsymbol{\zeta},\\ P_4 &= -\boldsymbol{\xi}^{\intercal} M\left(\boldsymbol{y}^{(0)}+\boldsymbol{y}^{(2)}\right) - \frac{1}{4}\boldsymbol{\xi}^{\intercal} N\begin{pmatrix}(L_2^{-1}M\boldsymbol{\eta})_1 & 0\\ (L_2^{-1}M\boldsymbol{\eta})_2 & (L_2^{-1}M\boldsymbol{\eta})_1\\ 0 & (L_2^{-1}M\boldsymbol{\eta})_2\end{pmatrix} L_3^{-1} M L_2^{-1} M\boldsymbol{\eta},\\ P_5 &= 4\boldsymbol{\xi}^{\intercal} M L_2^{-1}\begin{pmatrix}1 & 0\\ 0 & \delta_0\end{pmatrix} L_2^{-1} M\boldsymbol{\eta}\,.\end{aligned}$$

Rearranging Eq. (C.1), we find

$$A_{\hat{T}} = A_{\hat{X}\hat{X}} + \hat{\delta}_2 A + \hat{\mu}_1 q_1 A|A|^2 - q_2 A|A|^4 + 2\hat{\mu}_1 i A_{\hat{X}} + q_3 i A^2 \bar{A}_{\hat{X}} + q_4 i A_{\hat{X}}|A|^2\,,$$

where

$$\begin{aligned}q_1 &= -\frac{1}{k_c^2(1-k_c^2)^2}\left(\frac{P_1}{\hat{\mu}_1} + (P_2+P_3)\sqrt{\frac{k_c^2(1-k_c^2)}{\delta_0}} + \sqrt{\delta_0 k_c^2(1-k_c^2)^3}\psi_1\right)\,,\\ q_2 &= \frac{1}{k_c^2(1-k_c^2)^2}((P_2+P_3)\psi_1 + P_4)\,,\\ q_3 &= -\sqrt{\frac{1}{\delta_0 k_c^2(1-k_c^2)^3}}\left(P_3 - \delta_0(1-k_c^2)\psi_1\right)\,,\\ q_4 &= -\frac{1}{2}\sqrt{\frac{1}{\delta_0 k_c^2(1-k_c^2)^3}}\left(P_5 - 2P_2 - 4\psi_1\delta_0(1-k_c^2)\right)\,.\end{aligned}$$

As a check on the algebra here, we observe that in the specific case in which $\boldsymbol{\xi}^{\intercal} M\boldsymbol{\eta} = 0$ we have $P_1 = P_4 = P_5 = 0$, and further simplifications yield precisely the same quintic Ginzburg–Landau equation as was derived in Appendix B.

Appendix D. Numerical simulations

For the numerical simulations, two example minimal schemes were selected: one from class **a** for which $K > 0$ and one from class **c** (for which $K = 0$), given below in schemes (D.1), (D.2) respectively. Since the diffusion terms are diagonal, the governing PDEs

$$\partial_t\begin{pmatrix}U\\V\end{pmatrix} = \left\{\begin{pmatrix}1 & 0\\ 0 & \delta\end{pmatrix}\nabla^2 + \begin{pmatrix}1 & -\mu\\ \mu & -\vartheta\end{pmatrix}\right\}\begin{pmatrix}U\\V\end{pmatrix} + N\begin{pmatrix}\frac{1}{2}U^2\\ UV\\ \frac{1}{2}V^2\end{pmatrix}\,,$$

are easily Fourier transformed in space:

$$\partial_t\begin{pmatrix}\tilde{U}_k\\ \tilde{V}_k\end{pmatrix} = \left\{-k^2\begin{pmatrix}1 & 0\\ 0 & \delta\end{pmatrix} + \begin{pmatrix}1 & -\mu\\ \mu & -\vartheta\end{pmatrix}\right\}\begin{pmatrix}\tilde{U}_k\\ \tilde{V}_k\end{pmatrix} + N\begin{pmatrix}\frac{1}{2}(\tilde{U}*\tilde{U})_k\\ (\tilde{U}*\tilde{V})_k\\ \frac{1}{2}(\tilde{V}*\tilde{V})_k\end{pmatrix}\,,$$

where $(\cdot\ *\ \cdot)$ denotes a convolution, and this transformed system is integrated numerically on a one-dimensional spatial domain $x \in [0, L]$ with periodic boundary conditions using a fifth-order Taylor approximation to Cox and Matthews' mETD4RK method [23], which has fourth-order accuracy. Following Kassam and Trefethen [24], it is simpler to evaluate the nonlinear terms in real space, and so the implementation of the numerical scheme becomes pseudospectral, with the diagonality of the diffusion terms being exploited to efficiently evaluate the linear terms in Fourier space. Code files are available from the Zenodo digital repository: doi:10.5281/zenodo.14185376.

D.1. Example from class **a**

The first example corresponds to the (pseudo-)reaction scheme

$$\begin{cases}\quad 2U \xrightarrow{r_1} 4U + 3V\\ U + V \xrightarrow{r_2} \emptyset\\ \quad \emptyset \xrightarrow{r_3} U\end{cases}\,, \tag{D.1}$$

with parameter values $(r_1, r_2, r_3) = (1, \frac{6}{5}, 1)$. We also fix the diffusivity of species U to be unity. Accordingly, the PDEs being integrated numerically are

$$\partial_t\begin{pmatrix}u\\ v\end{pmatrix} = \begin{pmatrix}1 & 0\\ 0 & D_2\end{pmatrix}\nabla^2\begin{pmatrix}u\\ v\end{pmatrix} + \begin{pmatrix}1 + 2u^2 - \frac{6}{5}uv\\ 3u^2 - \frac{6}{5}uv\end{pmatrix}\,,$$

or equivalently

$$\begin{aligned}\partial_t\begin{pmatrix}u-1\\ v-\frac{5}{2}\end{pmatrix} &= \left\{\begin{pmatrix}1 & 0\\ 0 & D_2\end{pmatrix}\nabla^2 + \begin{pmatrix}1 & -\frac{6}{5}\\ 3 & -\frac{6}{5}\end{pmatrix}\right\}\begin{pmatrix}u-1\\ v-\frac{5}{2}\end{pmatrix}\\ &\quad + \begin{pmatrix}4 & -\frac{6}{5}\\ 6 & -\frac{6}{5}\end{pmatrix}\begin{pmatrix}\frac{1}{2}(u-1)^2\\ (u-1)(v-\frac{5}{2})\end{pmatrix}\,,\end{aligned}$$

and the nondimensionalised form (19) is

$$\begin{aligned}\partial_t\begin{pmatrix}U\\ V\end{pmatrix} &= \left\{\begin{pmatrix}1 & 0\\ 0 & D_2\end{pmatrix}\nabla^2 + \begin{pmatrix}1 & -\frac{3}{5}\sqrt{10}\\ \frac{3}{5}\sqrt{10} & -\frac{6}{5}\end{pmatrix}\right\}\begin{pmatrix}U\\ V\end{pmatrix}\\ &\quad + \begin{pmatrix}4 & -\frac{3}{5}\sqrt{10}\\ \frac{6}{5}\sqrt{10} & -\frac{6}{5}\end{pmatrix}\begin{pmatrix}\frac{1}{2}U^2\\ UV\end{pmatrix}\,,\end{aligned}$$

where $U = u - 1$, $V = \frac{1}{5}\sqrt{10}(v - \frac{5}{2})$.

D.1.1. *Figs.* 4 *and* 5

To establish that the system can settle to a stable stripe pattern, the PDE system was integrated on a spatial domain $x \in [0, L]$ with $L = 27$ – being approximately three wavelengths of the critical instability mode – with periodic boundary conditions using a regular spatial mesh of 2^{10} nodes and a time step of 2^{-16}, initialised with

$$u(x,0) = u^* + \frac{1}{100}\cos(3\cdot\tfrac{2\pi x}{L})\ ,\ v(x,0) = v^*\ .$$

The diffusivity of the second species was chosen to be $D_2 = \frac{25}{2}$, where the instability threshold value is $\delta_0 = \frac{6}{5}(5+2\sqrt{6}) \approx 11.8788$. The resultant spatiotemporal profiles $u(x,t), v(x,t)$ are shown in Fig. 4. The time evolution of the Fourier mode amplitudes for the first species are shown in the left-hand plot of Fig. 5. The time evolution of the Fourier amplitude of the critical instability mode for both species is shown in the right-hand plot of Fig. 5. The linearised analysis predicts that at early times the growth rate of this mode will be

$$\lambda(k) = \frac{1}{20}\left(\sqrt{\left(115k^2+22\right)^2 - 1440} - 135k^2 - 2\right) \approx 0.02032\ ,$$

where the wavenumber is $k = \frac{2\pi}{9}$. The slope of the dashed line in Fig. 5 indicates this prediction.

D.1.2. *Fig. 9 – left-hand plot*

To investigate how the stripe amplitude scales with the diffusivity, the same system was simulated on the domain $x \in [0, L]$ now with $L = 6\pi/\sqrt{-2+\sqrt{6}}$ – being exactly three wavelengths of the critical instability mode – with periodic boundary conditions and the same initialisation of

$$u(x,0) = u^* + \frac{1}{100}\cos(3\cdot\tfrac{2\pi x}{L})\ ,\ v(x,0) = v^*\ ,$$

with different choices of the diffusivity $D_2 \in [\delta_0 + \exp(-5), \delta_0 + 1]$. If D_2 is chosen closer to the threshold, computation times increase exponentially; for D_2 much further from the threshold the asymptotic assumptions break down and our predictions lose accuracy. For efficiency, these repeat simulations were performed on a regular spatial mesh of only 2^7 nodes allowing a larger time step of 2^{-8}. High wavenumber modes of $k_e > 32$ were also filtered out. The simulations were run until the change in Fourier-transformed concentrations $\tilde{u}(k,t), \tilde{v}(k,t)$ between time steps was smaller than 10^{-8} in uniform norm, and the final amplitude of the 3-period Fourier mode was recorded. These final time amplitudes are shown on a log scale in the left-hand plot of Fig. 9. The weakly nonlinear analysis predicts, for a pattern of the critical waveform, a steady state amplitude

$$|A|^2 = \frac{k_c^2(1-k_c^2)^2}{K}\delta_2\ .$$

Evaluating for this case of class **a**, with our chosen parameter values, yields the steady state prediction

$$|A| = \left(\frac{25\left(-90+37\sqrt{6}\right)}{1368}\delta_2\right)^{\frac{1}{2}}\ .$$

The leading order asymptotics give

$$\begin{aligned}\begin{pmatrix}U\\V\end{pmatrix} &= \varepsilon(a+\bar{a})\boldsymbol{\eta} + \mathcal{O}(\varepsilon^2)\\ &= 2\varepsilon\cos(k_c x)A\boldsymbol{\eta} + \mathcal{O}(\varepsilon^2) \text{ assuming } A\in\mathbb{R}\ ,\end{aligned}$$

where $\varepsilon^2 = (\delta-\delta_0)/\delta_2$. Together then, we have the leading order prediction

$$|\tilde{u}_{k_c}| = \left(\frac{5\left(-90+37\sqrt{6}\right)}{19}\right)^{\frac{1}{2}}(\delta-\delta_0)^{\frac{1}{2}}\ ,$$

$$|\tilde{v}_{k_c}| = \frac{5}{6}(3-\sqrt{6})|\tilde{u}_{k_c}|\ .$$

The dashed lines in Fig. 9 plot this prediction.

D.2. *Example from class* **c**

The second example corresponds to the (pseudo-)reaction scheme

$$\begin{cases} 2U \xrightarrow{r_1} 4U+3V \\ U+V \xrightarrow{r_2} \emptyset \\ U \xrightarrow{r_3} 2U \end{cases}\ , \tag{D.2}$$

with parameter values $(r_1, r_2, r_3) = (1, 11/5, 1)$. Again we fix the diffusivity of species U to be unity. Accordingly, the PDEs being integrated numerically are

$$\partial_t\begin{pmatrix}u\\v\end{pmatrix} = \begin{pmatrix}1&0\\0&D_2\end{pmatrix}\nabla^2\begin{pmatrix}u\\v\end{pmatrix} + \begin{pmatrix}u+2u^2-\frac{11}{5}uv\\ 3u^2-\frac{11}{5}uv\end{pmatrix}\ ,$$

or equivalently

$$\begin{aligned}\partial_t\begin{pmatrix}u-1\\v-\frac{15}{11}\end{pmatrix} &= \left\{\begin{pmatrix}1&0\\0&D_2\end{pmatrix}\nabla^2 + \begin{pmatrix}2&-\frac{11}{5}\\3&-\frac{11}{5}\end{pmatrix}\right\}\begin{pmatrix}u-1\\v-\frac{15}{11}\end{pmatrix}\\ &\quad + \begin{pmatrix}4&-\frac{11}{5}\\6&-\frac{11}{5}\end{pmatrix}\begin{pmatrix}\frac{1}{2}(u-1)^2\\(u-1)(v-\frac{15}{11})\end{pmatrix}\ ,\end{aligned}$$

and the nondimensionalised form (19) analysed above is

$$\begin{aligned}\partial_{\hat{t}}\begin{pmatrix}U\\V\end{pmatrix} &= \left\{\begin{pmatrix}1&0\\0&D_2\end{pmatrix}\hat{\nabla}^2 + \begin{pmatrix}1&-\frac{1}{10}\sqrt{165}\\\frac{1}{10}\sqrt{165}&-\frac{11}{10}\end{pmatrix}\right\}\begin{pmatrix}U\\V\end{pmatrix}\\ &\quad + \begin{pmatrix}2&-\frac{1}{10}\sqrt{165}\\\frac{1}{5}\sqrt{165}&-\frac{11}{10}\end{pmatrix}\begin{pmatrix}\frac{1}{2}U^2\\UV\end{pmatrix}\ ,\end{aligned}$$

where $\hat{t} = 2t$, $\hat{x} = \sqrt{2}x$, $U = u-1$, $V = \frac{1}{15}\sqrt{165}\left(v-\frac{15}{11}\right)$.

D.2.1. *Figs. 6 and 7*

To establish that the system can settle to a stable stripe pattern, the PDE system was integrated on a spatial domain $x \in [0, L]$ with $L = 22$ – being approximately three wavelengths of the critical instability mode – with periodic boundary conditions using a regular spatial mesh of 2^{10} nodes and a time step of 2^{-16}, initialised with

$$u(x,0) = u^* + \frac{1}{100}\cos\left(3\cdot\tfrac{2\pi x}{L}\right)\ ,\ v(x,0) = v^*\ .$$

The diffusivity of the second species was chosen to be $D_2 = \frac{9}{2}$, where the instability threshold value is $\delta_0 = \frac{11}{10}(2+\sqrt{3}) \approx 4.1053$. The resultant spatiotemporal profiles $u(x,t), v(x,t)$ are shown in Fig. 6. The time evolution of the Fourier mode amplitudes for the first species are shown in the left-hand plot of Fig. 7. The time evolution of the Fourier amplitude of the critical instability mode for both species is shown in the right-hand plot of Fig. 7. The linearised analysis predicts that at early times the growth rate of this mode will be

$$\lambda(k) = \frac{1}{20}\left(\sqrt{\left(35k^2+42\right)^2 - 2640} - 55k^2 - 2\right) \approx 0.08486\ ,$$

where the wavenumber is $k = \frac{3\pi}{11}$. The slope of the dashed line in Fig. 7 indicates this prediction.

D.2.2. *Fig. 9– right-hand plot*

To investigate how the stripe amplitude scales with the diffusivity, the same system was simulated on the domain $x \in [0, 6\pi/\sqrt{-1+\sqrt{3}})$ – being exactly three wavelengths of the critical instability mode – with periodic boundary conditions and the same initialisation of

$$u(x,0) = u^* + \frac{1}{100}\cos\left(3\cdot\tfrac{2\pi x}{L}\right)\ ,\ v(x,0) = v^*\ ,$$

with different choices of the diffusivity $D_2 \in [\delta_0 + \exp(-7), \delta_0 + \exp(-2)]$. For efficiency, these repeat simulations were performed on a regular spatial mesh of only 2^7 nodes allowing a larger time step of 2^{-8}. High wavenumber modes of $k_e > 32$ were also filtered out. The simulations were run until the concentrations $u(x,t), v(x,t)$ had approximately reached stationarity and the final amplitude of the 3-period Fourier

mode was recorded. These final time amplitudes are shown on a log scale in the right-hand plot of Fig. 9. The weakly nonlinear analysis predicts, for a pattern of the critical waveform, a steady state amplitude

$$|A|^4 = \frac{9(\delta_0 - \vartheta)^3(\delta_0 + \vartheta)}{100\chi_1^4\delta_0^5}\delta_2 \ ,$$

which, evaluating for this case of class **c**, with our chosen parameter values, yields the steady state prediction

$$|A| = \left(\frac{40\left(-3+2\sqrt{3}\right)}{1331}\delta_2\right)^{\frac{1}{4}} \ .$$

The leading order asymptotics give

$$\begin{pmatrix} U \\ V \end{pmatrix} = \varepsilon^{\frac{1}{2}}(a+\bar{a})\boldsymbol{\eta} + \mathcal{O}(\varepsilon)$$
$$= 2\varepsilon^{\frac{1}{2}}\cos(k_c x)A\boldsymbol{\eta} + \mathcal{O}(\varepsilon) \text{ assuming } A \in \mathbb{R} \ ,$$

where $\epsilon^2 = (\delta - \delta_0)/\delta_2$. Together then, we have the leading order prediction

$$|\tilde{u}_{k_c}| = \left(\frac{72\left(-3+2\sqrt{3}\right)}{55}\right)^{\frac{1}{4}}(\delta-\delta_0)^{\frac{1}{4}} \ , \tag{D.3a}$$

$$|\tilde{v}_{k_c}| = \frac{5}{11}(3-\sqrt{3})|\tilde{u}_{k_c}| \ . \tag{D.3b}$$

The dashed lines in Fig. 9 plot this prediction. We can even pull out the first correction to predictions (D.3) by including terms up to $\mathcal{O}(\varepsilon^{3/2})$. Assuming $A \in \mathbb{R}$ and A to be independent of X, we have

$$\begin{pmatrix} \tilde{U}_{k_c} \\ \tilde{V}_{k_c} \end{pmatrix} = 2\varepsilon^{\frac{1}{2}}A\boldsymbol{\eta} + \frac{5}{3}\frac{\chi_1^2}{k_c^2}\varepsilon^{\frac{3}{2}}A^3(\boldsymbol{\zeta} + c\boldsymbol{\eta}) + \mathcal{O}(\varepsilon^{\frac{5}{2}}) \ ,$$

where c is some constant that could be determined by continuing our analysis to higher orders in ε. For our purposes, we simply estimate c based on the output of the numerical simulations. Evaluating $\chi_1, k_c^2, \boldsymbol{\eta}, \boldsymbol{\zeta}$ for the particular parameter values of our simulation and transforming this back in terms of u and v we get

$$|\tilde{u}_{k_c}| = \left(\frac{72\left(-3+2\sqrt{3}\right)}{55}(\delta-\delta_0)\right)^{\frac{1}{4}}$$
$$\times \left|1 + (2-\sqrt{3})\left(\frac{75}{121}\right)^{\frac{1}{4}}\left(\frac{10(63-\sqrt{3})}{2973} + c\right)(\delta-\delta_0)^{\frac{1}{2}}\right| \ ,$$

$$|\tilde{v}_{k_c}| = \left(\frac{72\left(-3+2\sqrt{3}\right)}{55}(\delta-\delta_0)\right)^{\frac{1}{4}} \cdot \frac{5}{11}(3-\sqrt{3})$$
$$\times \left|1 - (2-\sqrt{3})\left(\frac{75}{121}\right)^{\frac{1}{4}}\left(\frac{11(123+61\sqrt{3})}{2973} - c\right)(\delta-\delta_0)^{\frac{1}{2}}\right| \ .$$

Through a process of trial and improvement, we can find a suitable value for c in order that the error in the prediction is reduced from $\mathcal{O}((\delta-\delta_0)^{3/4})$ to $\mathcal{O}((\delta-\delta_0)^{5/4})$.

Data availability

Data will be made available on request.

References

[1] A.M. Turing, The chemical basis of morphogenesis, Phil. Trans. R. Soc. Lond. B 237 (1952) 37–72.
[2] J.D. Murray, Mathematical Biology II : Spatial Models and Biomedical Applications, third ed., in: Interdisciplinary Applied Mathematics, vol. 18, Springer, New York, N.Y., 2003.
[3] R. Hoyle, Pattern Formation: An Introduction to Methods, Cambridge University Press, Cambridge, 2006.
[4] M.C. Cross, H. Greenside, Pattern Formation and Dynamics in Nonequilibrium Systems, Cambridge University Press, Cambridge, UK, 2009.
[5] L.M. Pismen, Patterns and Interfaces in Dissipative Dynamics : Revised and Extended, Now also Covering Patterns of Active Matter, second ed., in: Springer Series in Synergetics, Springer International Publishing: Imprint: Springer, Cham, Switzerland, 2023.
[6] A. Gierer, H. Meinhardt, A theory of biological pattern formation, Kybernetik 12 (1) (1972) 30–39.
[7] I. Prigogine, R. Lefever, Symmetry breaking instabilities in dissipative systems. II, J. Chem. Phys. 48 (4) (1968) 1695–1700.
[8] J. Schnakenberg, Simple chemical reaction systems with limit cycle behaviour, J. Theoret. Biol. 81 (3) (1979) 389–400.
[9] P. Gray, S.K. Scott, Sustained oscillations and other exotic patterns of behavior in isothermal reactions, J. Phys. Chem. 89 (1) (1985) 22–32.
[10] S.A. Levin, L.A. Segel, Hypothesis for origin of planktonic patchiness, Nature 259 (5545) (1976) 659.
[11] T.E. Woolley, A.L. Krause, E.A. Gaffney, Bespoke turing systems, Bull. Math. Biol. 83 (5) (2021) 41.
[12] F.R. Waters, C.A. Yates, J.H.P. Dawes, Minimal reaction schemes for pattern formation, J. R. Soc. Interface 21 (211) (2024) 20230490.
[13] V. Rottschäfer, A. Doelman, On the transition from the Ginzburg–Landau equation to the extended Fisher–Kolmogorov equation, Physica D 118 (3) (1998) 261–292.
[14] M.C. Cross, P.C. Hohenberg, Pattern formation outside of equilibrium, Rev. Modern Phys. 65 (1993) 851–1112.
[15] L.A. Segel, Distant side-walls cause slow amplitude modulation of cellular convection, J. Fluid Mech. 38 (1) (1969) 203–224.
[16] A.C. Newell, J.A. Whitehead, Finite bandwidth, finite amplitude convection, J. Fluid Mech. 38 (2) (1969) 279–303.
[17] J.T. Stuart, On the non-linear mechanics of hydrodynamic stability, J. Fluid Mech. 4 (1) (1958) 1–21.
[18] J.T. Stuart, On the non-linear mechanics of wave disturbances in stable and unstable parallel flows Part 1. The basic behaviour in plane Poiseuille flow, J. Fluid Mech. 9 (3) (1960) 353–370.
[19] Y. Kuramoto, Chemical Oscillations, Waves, and Turbulence, Springer Series in Synergetics, Springer, Berlin, Heidelberg, 1984.
[20] E.P. Zemskov, V.K. Vanag, I.R. Epstein, Amplitude equations for reaction-diffusion systems with cross diffusion, Phys. Rev. E 84 (3) (2011) 036216.
[21] K. Wang, M.L. Steyn-Ross, D.A. Steyn-Ross, M.T. Wilson, Derivation of the amplitude equation for reaction–diffusion systems via computer-aided multiple-scale expansion, Int. J. Bifurcation Chaos 24 (07) (2014) 1450101.
[22] E. Villar-Sepúlveda, A. Champneys, Computation of turing bifurcation normal form for n-component reaction-diffusion systems, ACM Trans. Math. Software 49 (4) (2023) 35:1–35:24.
[23] S.M. Cox, P.C. Matthews, Exponential time differencing for stiff systems, J. Comput. Phys. 176 (2) (2002) 430–455.
[24] A.-K. Kassam, L.N. Trefethen, Fourth-order time-stepping for stiff PDEs, SIAM J. Sci. Comput. 26 (4) (2005) 1214–1233.
[25] H.-C. Kao, E. Knobloch, Weakly subcritical stationary patterns: Eckhaus instability and homoclinic snaking, Phys. Rev. E 85 (2) (2012) 026211.